IEEE Open Journal of Vehicular Technology

Received XX Month, XXXX; revised XX Month, XXXX; accepted XX Month, XXXX; Date of publication XX Month, XXXX; date of current version 27 June, 2024.

Digital Object Identifier 10.1109/OJVT.2024.0627000

Optimizing Small Cell Performance: A New MIMO Paradigm with Distributed ASTAR-RISs

Shakil Ahmed[1] ***(Member, IEEE)***, **Ahmed E. Kamal**[1] ***(Fellow, IEEE)***, **Mohamed Y. Selim**[1], ***(Senior Member, IEEE)***, **Md Akbar Hossain**[2], ***(Senior Member, IEEE)*** **and Saifur Rahman Sabuj**[3], ***(Senior Member, IEEE)***

[1]Department of Electrical and Computer Engineering, Iowa State University, Ames, Iowa, USA.
[2]School of Computing, Eastern Institute of Technology, Auckland 1010, New Zealand.
[3]Department of Electrical and Electronic Engineering, Brac University, Dhaka 1212, Bangladesh.

CORRESPONDING AUTHOR: S. Ahmed (e-mail: shakil@iastate.edu) and M. A. Hossain (ahossain@eit.ac.nz)

ABSTRACT As the demand for high-speed data transmission grows with the expected emergence of 6G networks and the proliferation of wireless devices, more than traditional wireless infrastructure may be required. Small cell networks (ScNs) integrated with reconfigurable intelligent surfaces (RISs) and multiple-input-multiple-output (MIMO) have emerged as promising solutions to address this issue. However, ScNs have resource allocation limitations, and traditional RISs can only reflect signals in a limited propagation space of 180^0 with fixed reflection properties. This paper proposes a novel approach to overcome these challenges by introducing actively simultaneously transmitting and reflecting (ASTAR)-RISs. Unlike conventional RIS, ASTAR-RISs actively amplify and transmit signals, effectively mitigating the limited propagation challenge and improving signal strength, especially in dense ScNs. This approach enhances the quality of service in complex channel environments by amplifying, on top of reflection, from the macro base station (mBS), improving the overall signal strength, and providing 360^0 flexible propagation space. Furthermore, ASTAR-RIS enables dynamic beam management, significantly improving signal coverage and interference management, which are crucial in dense deployments. In this work, we propose a network architecture where distributed ASTAR-RIS units are deployed to assist small cell mBSs by optimizing signal coverage and enhancing communication performance. ASTAR-RISs dynamically control signal reflection and amplification, complementing the functionality of traditional small-cell BSs in dense network environments. Using the MIMO technique, we design phase shifts for ASTAR elements and develop optimal hybrid beamforming for users at the mBS. We dynamically control the ON/OFF status of the ASTAR-RIS based on active or idle status. We propose an efficient model that ensures fairness of signal-to-noise ratio (SNR) for all users and minimizes overall power consumption while meeting user SNR and phase shift constraints. To this end, we integrate robust beamforming and power allocation strategies, ensuring the system maintains reliable performance even under imperfect channel state information (CSI). We formulate a max-min optimization problem that optimizes the SNR and power consumption, subject to the ON/OFF status, phase shift, and power budget of the ASTAR-RIS. Our proposed method uses an alternating optimization algorithm to optimize the phase shift matrix at the ASTAR-RIS and the hybrid beamforming at the mBS. The approach includes two transmission schemes, and the phase optimization problem is solved using a successive convex approximation method that offers a closed-form solution at each step. Additionally, we use the dual method to determine the optimal ON/OFF status of the ASTAR-RIS. Comprehensive simulations validate the robustness and scalability of our proposed solution, particularly under varying network densities and CSI uncertainties. provides significant performance improvements over 170% compared to traditional RIS schemes.

INDEX TERMS Actively simultaneously transmitting and reflecting reconfigurable intelligent surfaces, hybrid beamforming, multiple-input-multiple-output, small cell networks

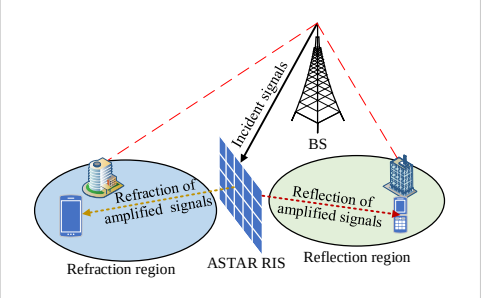

FIGURE 1: Operating Principle of ASTAR-RIS in ScNs

I. Introduction

THE current research thrust is to develop 6G technology, which is expected to be a transformative innovation set to revolutionize connectivity and reshape our world. With speeds up to 100 times faster than 5G, 6G will enable unprecedented levels of data transfer, ultra-low latency, massive device connectivity, unlocking new applications, and previously unimaginable opportunities [1]. Network densification is crucial to increasing overall network capacity to support the exponential growth of data traffic. One of the key elements in achieving this goal is the integration of multiple-input-multiple-output (MIMO) technology and the deployment of cost-effective small cell networks (ScNs) with wireless backhauling, which provide on-demand connectivity to users [2]. ScNs are low-cost radio access points with a small radio frequency (RF) power output and coverage range.

To understand the importance of ScNs and MIMO technology, we must first explore how they can be integrated to meet the requirements of 6G. While ScNs are crucial for increasing network capacity and providing cost-effective connectivity to ground users, there are still limitations to ScNs that need to be addressed, such as limited coverage area and backhaul capacity. MIMO technology with hybrid beamforming can be integrated to overcome these limitations to enhance spectral efficiency, signal quality, coverage, and network capacity. However, integrating MIMO with beamforming technologies in ScNs can be challenging. Mainly, channel modeling using MIMO in ScNs for 6G is not straightforward due to the ultra-dense deployment of ScNs, higher operating frequencies, and the small form factor of ScNs. Accurate and advanced channel modeling is crucial to overcome the limitations and ensure ScNs' successful deployment and operation in 6G. In addition to the challenges mentioned earlier, deploying ScNs with MIMO technology may need to compromise with excessive energy consumption. Using multiple antennas and advanced signal processing techniques can increase the energy consumption of ScNs, which can be problematic in scenarios where the power supply is limited, such as in remote or rural areas. Moreover, deploying large numbers of ScNs with MIMO technology can increase the overall energy consumption of the network.

Reconfigurable intelligent surfaces (RISs) have emerged as a promising technology to overcome the challenges faced by ScNs and revolutionize the way wireless communication networks may operate in 6G. With their meta-surface architecture, low energy consumption, and dynamic incident signal controlling capabilities, RISs have the potential to improve the capacity and coverage of ScNs significantly. By enhancing wireless signal quality and extending coverage, RISs can improve the efficiency of beamforming techniques and optimize the signal-to-noise ratio (SNR) at the receiver. They can also facilitate the creation of new network architectures that provide users with seamless connectivity and a higher quality of service (QoS). Overall, RISs are highly promising for enhancing the capacity and coverage of ScNs in 6G and may be a game-changer in designing the channel gain for the future of wireless communication [3].

RIS is a transformative technology for future wireless networks, capable of smartly manipulating electromagnetic waves. This capability is critical in unifying far-field and near-field communications, foundational to deploying B5G/6G networks. Far-field communications have traditionally dominated wireless systems, but as we advance into higher frequency bands like millimeter-wave and terahertz, near-field effects become more pronounced and relevant [4], [5]. RIS can seamlessly bridge these two domains by dynamically adjusting wavefronts to optimize signal strength and directionality at varying distances. Our research further explores the deployment of ASTAR-RIS in such scenarios, emphasizing its dual capability in active transmission and reflection. It is pivotal for environments where both range and precision are demanded.

Regrettably, conventional RISs cover only half of the propagation space, equivalent to 180^0. This may leave many users on the other half of the space out of service. Due to geographical constraints, this limitation can cause practical issues when the terminals are not located on both sides of the RISs. A recent concept has been introduced to address this problem, known as simultaneously transmitting and reflecting (STAR)-RIS [6]. It enables the splitting of signals into two regions, the transmission and reflection regions, while also permitting simultaneous reflection and refraction of signals incident on the surface. Specifically, when a signal reaches a specific element from either side of the surface, a portion of the incident power is refracted towards the opposite side and reflected towards the same side. The performance of STAR-RIS may not be optimal in dynamic and complex channel conditions with higher SNR since all the existing literature focuses on designing the reflection properties of passive elements [6]–[11]. However, research has yet to be conducted to address these limitations of STAR-RIS. However, the assumption of no interference between multiple cells oversimplifies real-world scenarios. Interference management is critical in multi-cell

This work is licensed under a Creative Commons Attribution 4.0 License. For more information, see https://creativecommons.org/licenses/by/4.0/

environments where inter-cell interference can significantly degrade system performance. By considering a single-cell model without interference, the network dynamics in larger multi-cell deployments are overlooked, reducing the practical applicability of the proposed solution. Therefore, this work incorporates additional interference modeling to represent realistic multi-cell scenarios better, offering a more comprehensive performance analysis. Moreover, the main difference between active and passive RIS lies in the amplification capabilities of active RIS, which inevitably leads to increased power consumption. It is crucial to acknowledge that the energy consumption of active RIS depends on the amplification coefficient. The initial assumptions in this study that overlook the direct relationship between energy consumption and the amplification factor are oversimplified. To address this, we revise our model to include a realistic energy consumption model for active RIS that explicitly accounts for the amplification coefficient, ensuring alignment with the physical characteristics of active RIS technologies.

Although RIS and STAR-RIS technologies have shown promise in improving wireless communication, they come with notable limitations regarding passive and fixed reflection properties, which this paper seeks to overcome. In this paper, we bridge the research gap by adding active properties on top of reflection and introducing a novel concept, the actively simultaneously transmitting and reflecting (ASTAR)-RIS panel to ScNs. The basic working principle of an ASTAR-RIS is shown in Fig. 1. It can improve efficiency in ScNs by reducing path loss and energy consumption. Moreover, the SNR can be increased without increasing the transmission power. In addition, ASTAR-RIS can be used to optimize the deployment of ScNs in a given area, which can further reduce energy consumption. However, it is essential to note that when RISs are in operation, they also require energy for signal control. Therefore, keeping the RISs OFF when not engaged in communications is crucial to achieving optimal efficiency. However, there is a trade-off between maximizing efficiency and the optimal functionality of the network. There are many strategies for controlling the sleep cycle of nodes, with dynamic sleeping modes being of current interest as they are based on the traffic and density of the network. Dynamic strategies can be controlled by the access point, user, or network, with each option offering advantages and disadvantages.

A. Recent Work and Motivations

There has been extensive research on ScNs in recent years to address various challenges, such as including time-division multiple access scheduling [12], [13], orthogonal frequency-division multiple access scheduling [14], fractional frequency reuse [15], and power control [16]. A multi-domain management scheme optimizing scheduling and power was proposed in [17]. Another approach to address the power consumption issue in ScNs is selectively putting some BSs to sleep while maintaining the QoS for users [18]. Researchers have also proposed various algorithms to optimize ScNs performance, including subcarrier allocation [19]. Additionally, spatial multiplexing in non-cooperative two-tier networks has been explored [20].

Recent studies have emphasized the potential of RIS technology, including STAR-RIS, as a key enabler for next-generation networks. The STAR-RIS concept was introduced in [10], [11] and further validated through prototype implementations by NTT DOCOMO [21]. STAR-RISs offer a unique advantage by simultaneously transmitting and reflecting incident signals. Other significant implementations include manipulating transmission and reflection via graphene-based dynamic metasurfaces [22] and multi-layer metasurfaces [23]. Coverage optimization in STAR-RIS-supported NOMA and orthogonal multiple access systems was studied in [24]. Moreover, RIS technology applications in indoor multi-user downlink communication systems have been studied, optimizing analog and digital beamforming to maximize total system rates [24]. A branch-and-bound algorithm was developed for finite set phase shift designs in RIS [25], while other studies focused on minimizing total transmit power for MIMO RIS-assisted NOMA systems [26]–[28].

Further research explored optimization techniques for outage probability in multiple RIS-assisted systems [29], maximizing received power in downlink millimeter-wave communications [30], and designing double-hop RIS-assisted systems [31]. In multi-cell networks with NOMA, joint optimization for multi-RIS-assisted full-duplex systems was investigated [32]. However, energy efficiency remains a concern, as RISs consume power during signal control [33]–[36]. In addition, recent advancements have focused on optimizing RIS performance through joint resource allocation and system design [37]. Particularly, solutions targeting hybrid beamforming in RIS-assisted networks have been proposed [38], demonstrating improvements in spectral efficiency and energy savings. Despite these advances, the potential of integrating ASTAR-RIS with MIMO technology remains unexplored.

While previous research has explored various aspects of RIS technology, including STAR-RIS applications, phase shift optimization, and energy efficiency [10], [11], [24], [33], our work is distinct in its focus on ASTAR-RIS-assisted ScNs with MIMO technology, which has not been previously addressed in the literature. Unlike traditional passive or STAR-RIS systems, which only reflect or passively split signals, the proposed ASTAR-RIS system actively amplifies, reflects, and transmits signals simultaneously, significantly improving performance and energy efficiency. Additionally, our approach uniquely integrates dynamic ON/OFF control of ASTAR-RIS elements, optimizing energy consumption by deactivating idle elements, an aspect overlooked in prior studies. Furthermore, we introduce a novel hybrid beamforming design for ScNs, which optimizes the ASTAR-RIS phase shifts and the mBS beamforming to minimize power

consumption and maximize SNR. By leveraging a successive SCA method and dual optimization techniques, we provide a comprehensive solution that enhances the overall efficiency of ScNs, demonstrating a 170% improvement in network performance compared to conventional RIS systems. These contributions, especially integrating ASTAR-RIS with hybrid beamforming and energy-efficient control mechanisms, differentiate this work from existing studies.

B. Contribution

This study investigates the efficiency of ASTAR-RIS-assisted ScNs using MIMO and designs optimal hybrid beamforming and ASTAR-RIS phase shifts. To summarize, the contributions of this paper are as follows:

- We propose a novel distributed ASTAR-RIS-assisted ScNs in which an ASTAR-RIS serves multiple micro users in transmission and reflection regions. Our work proposes using distributed ASTAR-RIS technology to overcome the challenges of unstable links and blocked communications between nodes in next-generation wireless networks by reflecting, transmitting, and amplifying incoming signals simultaneously, making it a promising solution to improve the performance of ScNs.
- Our approach aims to maximize the network's efficiency by dynamically controlling each ASTAR-RIS's ON/OFF status and optimizing the reflection coefficient matrix. We also consider the energy consumption of all nodes, including the ASTAR-RIS. Furthermore, we introduce a binary variable to determine if the ASTAR-RISs are active or turned OFF when idle, leading to significant energy savings. Although RISs lack an amplifier and consequently result in lower gain, our study demonstrates that higher performance and significant energy savings can be achieved by appropriately designing the phase shifts of ASTAR-RISs and optimizing the energy consumption of all nodes.
- Proposed phase shift design adjusts the reflected signals' phase at each ASTAR element, steering the signal toward the desired receiver to enhance signal strength. Our study aims to minimize the network's overall power consumption and maximize the SNR while satisfying user rate, power budget, and ASTAR-RIS ON/OFF status constraints. To achieve this, we optimize the phase shift matrix of the ASTAR-RIS and the hybrid beamforming of the macro BS (mBS). We present two transmission schemes and formulate an optimization problem to design the ASTAR-RIS phase shift and hybrid beamforming. We use a successive convex approximation (SCA) method to solve the phase optimization problem, providing a closed-form solution at each step. Additionally, we use the dual method to determine the optimal ASTAR-RIS ON/OFF.
- By analyzing the simulation results, we illustrate that our proposed approach outperforms the conventional RIS regarding efficiency, yielding over 170% improvements. The findings reveal that optimizing the phase shifts applied by the ASTAR-RIS and hybrid beamforming results in better ScNs' performance.

TABLE 1: List of symbols used in the paper

Symbol	Definition	Symbol	Definition
L	ASTAR-RIS	K_t	Transmission users
N_l	Elements	α	Path loss exponent
d	Distance	K_r	Reflection users
k_m	macro user	$\mathbf{\Phi}^l_{k_r}$	Coefficient matrix
M	Antennas	$\mathbf{\Theta}^l_{k_t}$	Coefficient matrix
$\mathbf{g}_{k_m}$	Channel gain	$\mathbf{R}^{\text{los}}$	LOS component
$\mathbf{G}_l$	Channel gain	$\mathbf{R}^{\text{nlos}}$	NLOS component
$\mathbf{h}_{lk_r}$	Channel gain	β_p	Large scale path loss
Υ	Rician factor	$\theta^l_{k_t}, \theta^l_{k_r}$	Phase shift
$\beta^l_{k_t}, \beta^l_{k_r}$	Amplitude	x_l	Binary variables
$s_{k_t}, s^{nl}_{k_r}$	Signals	$\mathbf{w}_{\{\cdot\}}$	Beamforming
$p_{k_{\{t,r,m\}}}$	Circuit power	p_b	mBS circuit power
$\gamma_{\{\cdot\}}$	SNR	p_{RIS}	RIS power consumption
$\mathbf{g}_{k_t}$	Channel gain	$\mathbf{g}_{k_r}$	Channel gain
R	RF chain	ζ	Variable
$\mathbf{g}_{\{k_t,k_r\}}$	Gain	p_{k_t,k_r}	Transmit power
$\mathbf{\Delta}_{\{k_t,k_r\}}$	Variable	$\mathbf{V}$	Analog beamforming
$\mathbf{Y}_{\{k_t,k_r\}}$	Signals	$\mathbf{w}_{\{k_t,k_r,k_m\}}$	Digital beamforming

C. Mathematical Notations

The scalar is defined as a, the vector as $\mathbf{a}$, and the matrix as $\mathbf{A}$. A diagonal matrix with diagonal components is denoted by $\text{diag}\,(\cdot)$. The notation $[\boldsymbol{y}]_n$ indicates the n-th element of vector $\boldsymbol{y}$, whereas $[\mathbf{y}]_{kn}$ denotes the (k,n)-th element of matrix $\mathbf{y}$. Euclidean norm of vector $\boldsymbol{y}$ is represented by $|\boldsymbol{y}|$. The notation $\mathcal{CN}(y,\sigma)$ represents the distribution of a complex circularly symmetric Gaussian variable having a mean of y and a covariance of σ. Vector $\boldsymbol{y}$ conjugate is denoted by $\boldsymbol{y}^*$, its transpose is denoted by $\boldsymbol{y}^T$, and its conjugate transpose is denoted by $\boldsymbol{y}^H$. The real and imaginary components of a complex number x can be denoted as $\mathcal{R}(y)$ and $\mathcal{I}(y)$, respectively.

II. Proposed System Model

A. Scenario Description

We investigate the use of ASTAR-RISs in ScNs, considering a downlink transmission and MIMO. The network comprises an mBS for widespread wireless coverage, L number of ASTAR-RISs, where $l = 1, 2, ..., L$ refers to ASTAR-RIS, l. Our study assumes that the ASTAR-RISs, L are distributed. ASTAR-RIS, l, serves a single ScN and has N_l number of elements, where $n_l = 1, 2, ..., N_l$, refers to the elements in the ASTAR-RIS panel, l. Each ScN uses a unique resource block to prevent interference during data transmission. However, in a multi-cell scenario, signals from neighboring cells

This article has been accepted for publication in IEEE Open Journal of Vehicular Technology. This is the author's version which has not been fully edited and content may change prior to final publication. Citation information: DOI 10.1109/OJVT.2024.3509736 IEEE Open Journal of Vehicular Technology

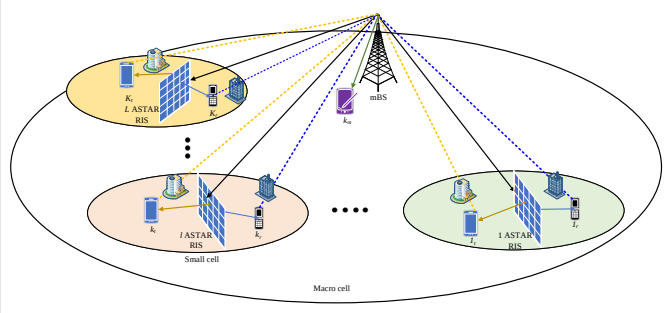

FIGURE 2: Proposed system model

can interfere with users in a given cell, leading to inter-cell interference. This interference must be mitigated to ensure robust system performance. The network has three types of users: transmission, reflection, and macro. The transmission and reflection users reside in the transmission and reflection regions of ASTAR-RIS, respectively. Assuming that multiple users in the network require data streams to be transmitted from the mBS, we employ a sub-connected hybrid beamforming structure with R number of RF chains.

The transmission users are numbered as K_t, where $k_t = 1, 2, ..., K_t$. The reflection users are numbered K_r, where $k_r = 1, 2, ..., K_r$. The mBS serves the macro user, denoted as k_m, without any assistance of ASTAR-RIS. We assume that mBS has M antennas that are uniformly arranged in a linear array, while each user in macro, transmission, and reflection regions is equipped with only one antenna.

In this work, we explicitly model inter-cell interference to capture the impact of signals transmitted by mBSs in neighboring cells. These interfering signals are particularly relevant in dense deployments, where adjacent cells have overlapping coverage areas. The interference differentiates the multi-cell system from a single-cell setup, affecting each user's signal-to-interference-plus-noise ratio (SINR). As depicted in Fig. 2, each ScN contains multiple users, situated in both the transmission and reflection regions of the ASTAR-RIS. Our proposed model aims to create an efficient network that supports users in the ScN transmission and reflection regions. This model presents a promising effective wireless network deployment solution by optimizing the ASTAR-RIS phase shift and hybrid beamforming. The symbols utilized in the paper are listed in Table I.

B. Channel Modeling

Tall obstacles are assumed to obstruct the line-of-sight link between the mBS and the reflection and transmission region users. We, therefore, model the channel propagation through the ASTAR-RIS, l for k_t and k_r. We consider macro user, k_m, can communicate with the mBS using line-of-sight links, saving the resource from ASTAR-RIS. We define the channel gains from mBS to k_m as $\mathbf{g}_{k_m} \in \mathbb{C}^{1\times R}$, mBS to k_t as $\mathbf{g}_t \in \mathbb{C}^{1\times R}$, mBS to k_r as $\mathbf{g}_r \in \mathbb{C}^{1\times R}$, mBS to ASTAR-RIS, l as $\mathbf{G}_l \in \mathbb{C}^{N_l\times M}$, ASTAR-RIS, l to user k_r (at reflection region) as $\mathbf{h}_{lk_r} \in \mathbb{C}^{1\times N_l}$, and ASTAR-RIS, l to user k_t (at transmission region) as $\mathbf{h}_{lk_t} \in \mathbb{C}^{1\times N_l}$.

We use the block flat-fading based-channel modeling throughout the paper. The definition of the large-scale path loss is provided in [39] as follows:

$$\beta_p = \frac{10^{\frac{G_{tr}+G_{rc}-35.95}{10}} 10^{\frac{G_{tr}+G_{rc}-33.05}{10}}}{d^{\alpha}}, \tag{1}$$

where the antenna gains at transmitting and receiving nodes are G_{tr} and G_{rc}, respectively, while the variable d represents the distance between the communicating nodes. α defines the path loss exponent. The channel gains, such as $\mathbf{G}_l$, $\mathbf{h}_{lk_r}$, $\mathbf{h}_{lk_t}$, are modeled as Rician fading channels. In general, the channel gain from two communicating nodes is expressed as follows:

$$\tilde{\mathbf{R}} = \sqrt{\frac{\Upsilon}{1+\Upsilon}}\mathbf{R}^{\text{los}} + \sqrt{\frac{1}{1+\Upsilon}}\mathbf{R}^{\text{nlos}}, \tag{2}$$

where Rician factor, denoted by Υ, is defined along with the line-of-sight and non-line-of-sight components, represented by $\mathbf{R}^{\text{los}}$ and $\mathbf{R}^{\text{nlos}}$, respectively. Both components are modeled using complex Gaussian distribution $\mathcal{CN}(0, 1)$. While the optimization methods proposed in this work are non-parametric and do not strictly depend on a specific channel model, we include the channel model in this section to provide a complete description of the system setup, as recommended by previous studies [40], [41]. This model helps contextualize performance metrics such as SNR and energy efficiency, which are influenced by channel conditions like path loss and fading [42]. Including the channel model also aligns with established RIS literature, highlighting the importance of considering physical layer characteristics for real-world deployment. Additionally, this model is beneficial for interpreting practical metrics, enabling a better understanding of overall system performance. Readers primarily focused on the optimization framework may note that the methods are independent of the specific channel model. Thus, this section can be regarded as supplementary to the core analysis.

C. Properties of ASTAR-RIS

We define the diagonal coefficient matrix of ASTAR-RIS, l for transmission space user, k_t as follows:

$$\mathbf{\Theta}^{l}_{k_t} = \text{diag}\left(\beta^{1_l}_{k_t} e^{j\theta^{1_l}_{k_t}}, ..., \beta^{n_l}_{k_t} e^{j\theta^{n_l}_{k_t}}, ..., \beta^{N_l}_{k_t} e^{j\theta^{N_l}_{k_t}}\right) \quad (3)$$

where the amplitude and phase shift of ASTAR element n_l in $\mathbf{\Theta}^{l}_{k_t} \in \mathbb{C}^{N_l \times N_l}$ are defined as $1 \leq \beta^{n_l}_{k_t}$ and $\theta^{n_l}_{k_t} \in [0, 2\pi)$, respectively. Additionally, we define the diagonal coefficient matrix of the ASTAR-RIS for reflection space user k_r as:

$$\mathbf{\Theta}^{l}_{k_r} = \text{diag}\left(\beta^{1_l}_{k_r} e^{j\theta^{1_l}_{k_r}}, ..., \beta^{n_l}_{k_r} e^{j\theta^{n_l}_{k_r}}, ..., \beta^{N_l}_{k_r} e^{j\theta^{N_l}_{k_r}}\right) \quad (4)$$

where the amplitude and phase shift of n_l ASTAR element for the reflection space user k_r are represented by $\beta^{n_l}_{k_r}$ and $\theta^{n_l}_{k_r} \in [0, 2\pi)$, respectively. We define in the diagonal coefficient matrix $\mathbf{\Theta}^{l}_{k_r} \in \mathbb{C}^{N_l \times N_l}$. These adjustments are applied to the incident signals during reflection. We define s^{n_l} as the wireless incident signal to characterize the ASTAR-RIS feature. When a wireless signal reaches ASTAR element, n_l, the signal is divided into refracted and reflected signals as s_{k_t} and s_{k_r}, respectively. Recent research in [43] suggests that reflection and transmission properties of n_l are generally independent. The refracted signals by ASTAR-RIS, n_l element is modeled as follows [7]:

$$s_{k_t} = s^{n_l} \beta^{n_l}_{k_t} e^{j\theta^{n_l}_{k_t}} \quad (5)$$

Similarly, the reflected signals by ASTAR-RIS, n_l element is modeled as follows:

$$s_{k_r} = s^{n_l} \beta^{n_l}_{k_r} e^{j\theta^{n_l}_{k_r}} \quad (6)$$

The coupling between $\beta^{n_l}_{k_t}$ and $\beta^{n_l}_{k_r}$ is governed by the law of energy conservation [7]. We express the amplitude coefficient due to the transmission and reflection properties of the element, n_l, as follows:

$$2 \leq \beta^{n_l}_{k_t} + \beta^{n_l}_{k_r} \quad (7)$$

This paper investigates the correlation between the phase shift and amplitude during the transmission and reflection processes of ASTAR-RIS. We aim to establish a mathematical model that can be utilized to design and implement ASTAR-RIS for future applications. $\beta^{n_l}_{k_t}$ and $\beta^{n_l}_{k_r}$ is formulated as follows [8]:

$$\beta^{n_l}_{k_t} = \left(1 - \beta^{t}_{\text{min}}\right)\left(\frac{\sin(\theta^{n_l}_{k_t} - \vartheta) + 1}{2}\right)^{\alpha_s} + \beta^{t}_{\text{min}} \quad (8)$$

$$\beta^{n_l}_{k_r} = \left(1 - \beta^{r}_{\text{min}}\right)\left(\frac{\sin(\theta^{n_l}_{k_r} - \vartheta) + 1}{2}\right)^{\alpha_s} + \beta^{r}_{\text{min}} \quad (9)$$

We define β^{r}_{min} and β^{t}_{min} as having positive values as constants with minimum reflection and transmission amplitudes, respectively. These constants are also related to the specific circuit implementation. We also define ϑ as the e horizontal distance between $-\pi/2$ and $\beta^{t,r}_{\text{min}}$. The controlling of the function's step is defined as α_s. However, (8) and (9) can be transformed to ideal phase shift design with amplitude 1 when we choose $\beta^{r}_{\text{min}} = \beta^{t}_{\text{min}} = 1$ and $\alpha_s = 0$.

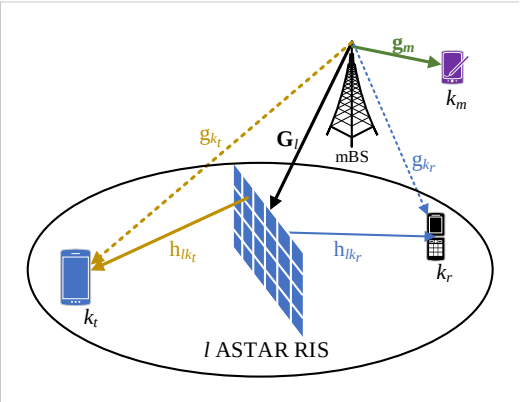

FIGURE 3: Gain demonstration of the proposed ScNs

D. Sleep Mode of ASTAR-RIS Panel

The deployment of ASTAR-RISs may consume a significant amount of energy. Moreover, keeping all the ASTAR elements active consumes additional amplification-related energy besides reflection and transmission-related energy. The introduction of active transmission is supported by recent advancements in metasurface technology, where active elements capable of both transmission and reflection have been demonstrated [41].The reflective and transmittance characteristics are also influenced by the accuracy of controlling the phase shifts of the elements and phase shifts' resolution. Besides optimizing the overall power consumption, any ASTAR-RIS may be turned OFF when idle; otherwise, it is ON. A binary variable, $x_l \in \{0, 1\}$ can determine if ASTAR-RIS, l is in the OFF $(x_l = 0)$ or in the ON mode $(x_l = 1)$.

III. Data Transmission

We employ the ASTAR-RIS to achieve optimal spatial coverage by simultaneously amplifying, reflecting, and transmitting the mBS transmit signals in ScNs to improve the data rate transmission. We assume the mBS knows the perfect channel state information (CSI) of all links. This assumption is standard in theoretical studies of RIS-based systems, especially in low-mobility user scenarios. It allows the system to optimize beamforming and phase shifts accurately. [44]. We design joint beamforming and phase shift using ASTAR-RIS for communication. The mBS can use hybrid beamforming to create multiple beams directed toward users within different resource blocks simultaneously, allowing the mBS to transmit signals to multiple users. By adjusting the amplitude and phase of signals in each beam, the mBS can steer the beams toward each user and optimize the transmission quality individually.

MIMO technology employs multiple antennas at the transmitter and a single antenna at the receiver to communicate with several users simultaneously. It enables the transmitter's multiple antennas to segregate the signals meant for different users and transmit them simultaneously, thereby boosting the network's overall capacity. Hybrid beamforming in STAR-

RIS-assisted ScNs may enable the transmission of multiple data streams simultaneously, resulting in improved spectral efficiency. Second, it reduces the hardware complexity of the system by using fewer RF chains. This is because hybrid beamforming combines analog and digital beamforming techniques, allowing for more efficient use of RF chains. Finally, it improves the signal quality by optimizing the beamforming weights and the phase shifts applied by the RIS, resulting in a higher SNR at the receiver.

We assume that $k_t \in K_t$, $k_r \in K_r$, and $k_m \in K_m$ require unique data streams. The signals intended for each user are independent and are denoted by s_{k_t}, s_{k_r}, and s_{k_m}, each satisfying the following conditions:

$$\mathbb{E}(|s_{k_t}|^2) = \mathbb{E}(|s_{k_r}|^2) = \mathbb{E}(|s_{k_m}|^2) = 1 \tag{10}$$

The signals are transmitted using hybrid beamforming techniques. First, each signal is weighted by a digital beamforming $\mathbf{w}_{k_t}, \mathbf{w}_{k_r}, \mathbf{w}_{k_m} \in \mathbb{C}^{R\times 1}$. Then, the resulting signal is multiplied by an analog beamforming $\mathbf{v}_r$ for each $r \in R$. The overall analog beamforming matrix is denoted by $\mathbf{V} \in \mathbb{C}^{M\times R}$, representing the entire analog beamforming structure. The possible phase shifts for ASTAR-RIS reflection coefficients for transmission and reflection users are defined as:

$$\mathcal{S}_l^t \triangleq \left\{ \beta_{k_t}^{n_l} e^{j\theta_{k_t}^{n_l}} \,\middle|\, \theta_{k_t}^{n_l} \in \left\{ 0, \frac{2\pi}{2^{\chi_1}}, \ldots, \frac{2\pi(2^{\chi_1}-1)}{2^{\chi_1}} \right\} \right\} \tag{11}$$

$$\mathcal{S}_l^r \triangleq \left\{ \beta_{k_r}^{n_l} e^{j\theta_{k_r}^{n_l}} \,\middle|\, \theta_{k_r}^{n_l} \in \left\{ 0, \frac{2\pi}{2^{\chi_2}}, \ldots, \frac{2\pi(2^{\chi_2}-1)}{2^{\chi_2}} \right\} \right\} \tag{12}$$

The received signals for the transmission, reflection, and macro users are given as follows:

$$\mathbf{y}_{k_t} = \mathbf{g}_{k_t} + x_l \mathbf{h}_{lk_t} \mathbf{\Theta}_{k_t}^l \mathbf{G}_l \mathbf{V} \mathbf{w}_{k_t} s_{k_t} + \sum_{i\neq \text{cell}} \mathbf{h}_{ki}^H \mathbf{w}_i s_i + n_{k_t} \tag{13}$$

$$\mathbf{y}_{k_r} = \mathbf{g}_{k_r} + x_l \mathbf{h}_{lk_r} \mathbf{\Theta}_{k_r}^l \mathbf{V} \mathbf{G}_l \mathbf{w}_{k_r} s_{k_r} + \sum_{i\neq \text{cell}} \mathbf{h}_{ki}^H \mathbf{w}_i s_i + n_{k_r} \tag{14}$$

$$\mathbf{y}_{k_m} = \mathbf{g}_{k_m} \mathbf{V} \mathbf{w}_{k_m} + \sum_{i\neq \text{cell}} \mathbf{h}_{ki}^H \mathbf{w}_i s_i + n_{k_m} \tag{15}$$

The terms $\sum_{i\neq \text{cell}} \mathbf{h}_{ki}^H \mathbf{w}_i s_i$ in each equation represent inter-cell interference, which arises from signals transmitted by neighboring mBSs. This interference directly impacts the SINR of users and differentiates the multi-cell scenario from single-cell systems. The resulting SINR expressions for each user type are as follows:

$$\gamma_{k_t} = \frac{\left| \mathbf{g}_{k_t} + \sum_{l=1}^{L} x_l \mathbf{h}_{lk_t} \mathbf{\Theta}_{k_t}^l \mathbf{G}_l \mathbf{V} \mathbf{w}_{k_t} s_{k_t} \right|^2}{\sum_{i\neq \text{cell}} |\mathbf{h}_{ki}^H \mathbf{w}_i s_i|^2 + \sigma_{k_t}^2} \tag{16}$$

$$\gamma_{k_r} = \frac{\left| \mathbf{g}_{k_r} + \sum_{l=1}^{L} x_l \mathbf{h}_{lk_r} \mathbf{\Theta}_{k_r}^l \mathbf{G}_l \mathbf{V} \mathbf{w}_{k_r} s_{k_r} \right|^2}{\sum_{i\neq \text{cell}} |\mathbf{h}_{ki}^H \mathbf{w}_i s_i|^2 + \sigma_{k_r}^2} \tag{17}$$

$$\gamma_{k_m} = \frac{|\mathbf{g}_{k_m} \mathbf{V} \mathbf{w}_{k_m}|^2}{\sum_{i\neq \text{cell}} |\mathbf{h}_{ki}^H \mathbf{w}_i s_i|^2 + \sigma_{k_m}^2} \tag{18}$$

These SINR expressions illustrate the impact of inter-cell interference on different types of users, emphasizing the importance of managing interference for improved system performance.

IV. Overall Power Consumption

The power consumption of the ASTAR-RIS-assisted ScNs includes the transmit power and circuit power of the mBS, the power of the ASTAR-RIS and its transmission and reflection circuits, and the power consumed by the macro users. Unlike passive RIS, ASTAR-RIS incorporates active signal amplification, leading to additional power consumption proportional to the amplification gain. Therefore, the total power consumption model must account for the amplification coefficient to provide a realistic assessment of the system's energy efficiency. Furthermore, our model incorporates a dynamic ON/OFF control mechanism that reduces power usage during idle periods, critical for improving energy efficiency in dense networks. These mechanisms ensure that our proposed scheme balances performance enhancements with increased energy demands.

1) Model for user power consumption

The power consumption of different types of users, such as macro, reflection, and transmission regions in terms of circuit power, can be expressed as follows:

$$p_u = p_{k_t} + p_{k_r} + p_{k_m} \tag{19}$$

where p_{k_t}, p_{k_r}, and p_{k_m} are the circuit power consumption of transmission, reflection, and macro users, respectively.

2) BS power consumption model

The power consumption due to the mBS signal transmission and circuit power is expressed as follows:

$$p_s = \frac{\mathbf{w}_{k_t}\mathbf{w}_{k_t}^H + \mathbf{w}_{k_r}\mathbf{w}_{k_r}^H + \mathbf{w}_{k_m}\mathbf{w}_{k_m}^H}{v} + p_b \tag{20}$$

where p_b is defined as the mBS circuit power. The power amplifier efficiency at the mBS is denoted by v.

3) Power consumption due to ASTAR-RIS

The power consumption of ASTAR-RIS, l, is expressed as follows:

$$p_l = \sum_{l=1}^{L} x_l N_l p_{\text{RIS}} + \sum_{l=1}^{L} \sum_{n_l=1}^{N_l} \eta_l |\beta_{n_l}|^2 \tag{21}$$

where p_{RIS} is a constant related to the power consumed during the transmission and reflection process, and x_l is the ON/OFF control variable for ASTAR-RIS, l. The additional

term $\eta_l|\beta_{n_l}|^2$ accounts for the power consumed due to amplification, where η_l represents the amplification efficiency and β_{n_l} denotes the amplification coefficient for element n_l of ASTAR-RIS, l. This term captures the increase in power consumption as a function of the amplification gain, addressing the distinction between active and passive RIS.

4) Overall power consumption

The total power consumption of the network is the sum of the power consumption of all nodes, which can be expressed as follows:

$$p_{\text{overall}} = p_u + p_s + p_l \tag{22}$$

This power model explicitly incorporates the amplification gain's impact on ASTAR-RIS power consumption, offering a more accurate and physically consistent evaluation of energy usage. The dynamic ON/OFF control ensures energy efficiency by deactivating unnecessary RIS elements during idle periods. While this study highlights the potential power-saving benefits of ASTAR-RIS, future work will extend this analysis to compare energy efficiency between active and passive RIS under varying amplification coefficients and network conditions. This comprehensive evaluation will provide deeper insights into the trade-offs between performance gains and energy consumption in real-world scenarios.

V. Problem Formulation

The objective of the optimization problem is to enhance the performance of ScNs with ASTAR-RIS by jointly optimizing the hybrid beamforming for reflection and transmission, ASTAR-RIS phase shift, and ON/OFF mode of the ASTAR-RIS while satisfying minimum SINR requirements, power budget, phase shift, and beamforming constraints. This formulation explicitly accounts for the increased power consumption associated with active amplification and incorporates inter-cell interference, ensuring a realistic and physically consistent model. The problem can be mathematically expressed as:

$$\max_{\substack{\zeta,\mathbf{w}_{k_t},\mathbf{w}_{k_r},\\ \boldsymbol{\theta}_{k_t},\boldsymbol{\theta}_{k_r},\boldsymbol{x}}} \left[\zeta - \iota\left(p_u + p_s + p_l + \sum_{l=1}^{L}\sum_{n_l=1}^{N_l}\eta_l|\beta_{n_l}|^2\right)\right] \tag{23a}$$

$$\text{s.t. } \mathbf{w}_{k_t}^H\mathbf{w}_{k_t} \le p_{\max},\ \mathbf{w}_{k_r}^H\mathbf{w}_{k_r} \le p_{\max} \tag{23b}$$

$$x_l \in \{0,1\}, \forall l \in \mathcal{L} \tag{23c}$$

$$\theta_{k_t}^l \in [0,2\pi],\ \theta_{k_r}^l \in [0,2\pi], \forall l \in \mathcal{L}, n_l \in \mathcal{N}_l \tag{23d}$$

$$\zeta \le \frac{\left|\mathbf{g}_{k_t} + \sum_{l=1}^{L} x_l \mathbf{h}_{lk_t}\boldsymbol{\Theta}_{k_t}^l\mathbf{G}_l\mathbf{V}\mathbf{w}_{k_t}s_{k_t}\right|^2}{\sum_{i\neq\text{cell}}|\mathbf{h}_{ki}^H\mathbf{w}_i s_i|^2 + \sigma_{k_t}^2}, \forall k_t \tag{23e}$$

$$\zeta \le \frac{\left|\mathbf{g}_{k_r} + \sum_{l=1}^{L} x_l \mathbf{h}_{lk_r}\boldsymbol{\Theta}_{k_r}^l\mathbf{G}_l\mathbf{V}\mathbf{w}_{k_r}s_{k_r}\right|^2}{\sum_{i\neq\text{cell}}|\mathbf{h}_{ki}^H\mathbf{w}_i s_i|^2 + \sigma_{k_r}^2}, \forall k_r \tag{23f}$$

We define $\boldsymbol{\theta}_{k_t} = [\theta_{k_t}^{11},\ldots,\theta_{k_t}^{1N_1},\ldots,\theta_{k_t}^{LN_L}]^T$, $\boldsymbol{\theta}_{k_r} = [\theta_{k_r}^{11},\ldots,\theta_{k_r}^{1N_1},\ldots,\theta_{k_r}^{LN_L}]^T$, and $\boldsymbol{x} = [x_1,\ldots,x_l,\ldots,x_L]^T$. The objective function in (23a) is a max-min problem, aiming to maximize fairness while considering the total network power consumption, including user, BS, and ASTAR-RIS components. The term $\sum_{l=1}^{L}\sum_{n_l=1}^{N_l}\eta_l|\beta_{n_l}|^2$ represents the power consumed by ASTAR-RIS due to active amplification, capturing the energy impact of amplification gain on power consumption. In (23b), we show the power budget for reflection and transmission phases, where $p_{\max}$ is the mBS maximum power budget. The ON/OFF mode of ASTAR-RIS is captured in (23c), where 0 defines the OFF and 1 the ON mode. Dynamic ON/OFF control ensures that ASTAR-RIS elements are only active when necessary, reducing energy consumption during idle periods. The phase shift constraint is shown in (23d). Constraints (23e) and (23f) include inter-cell interference terms $\sum_{i\neq\text{cell}}|\mathbf{h}_{ki}^H\mathbf{w}_i s_i|^2$, which capture the SINR degradation caused by neighboring cells' transmissions. These constraints ensure that SINR thresholds for transmission and reflection users are met under realistic interference conditions. The optimization problem (23) is a mixed-integer non-linear programming (MINLP) problem and is challenging to solve due to the coupling of variables. Due to this complexity, obtaining an optimal global solution of (23) is challenging. Two iterative algorithms are developed to find nearly optimal solutions for the optimization problem aimed at enhancing the performance of ASTAR-RIS-assisted wireless networks.

VI. Proposed Solution

Maximum ratio transmission (MRT) is a beamforming technique that aims to improve the receiver's SNR in wireless communication systems. It weights the transmitted signal by the conjugate of the channel coefficients. It normalizes it by the magnitude of the channel coefficients, ensuring that the transmitted signal is optimally aligned with the channel, improving signal quality. MRT is optimal when the receiver has perfect CSI. In this study, we use MRT to optimize the transmission of signals to different resource blocks, computing $\mathbf{w}_{k_t}$ and $\mathbf{w}_{k_r}$ accordingly. Unlike traditional beamforming techniques, the proposed method explicitly incorporates the impact of inter-cell interference and amplification power consumption. This ensures that the MRT design remains robust in multi-cell environments, where signals from neighboring cells can degrade the system's performance. We write the beamforming expressions for k_t and k_r as follows:

$$\mathbf{w}_{k_t} = \sqrt{p_{k_t}}\frac{\mathbf{g}_{k_t} + \sum_{l=1}^{L} x_l\mathbf{h}_{lk_t}\boldsymbol{\Theta}_{k_t}^l\mathbf{G}_l\mathbf{V}s_{k_t}}{\left|\mathbf{g}_{k_t} + \sum_{l=1}^{L} x_l\mathbf{h}_{lk_t}\boldsymbol{\Theta}_{k_t}^l\mathbf{G}_l\mathbf{V}s_{k_t}\right|} \tag{24}$$

$$\mathbf{w}_{k_r} = \sqrt{p_{k_r}}\frac{\mathbf{g}_{k_r} + \sum_{l=1}^{L} x_l\mathbf{h}_{lk_r}\boldsymbol{\Theta}_{k_r}^l\mathbf{G}_l\mathbf{V}s_{k_r}s_{k_t}}{\left|\mathbf{g}_{k_r} + \sum_{l=1}^{L} x_l\mathbf{h}_{lk_r}\boldsymbol{\Theta}_{k_r}^l\mathbf{G}_l\mathbf{V}s_{k_r}s_{k_t}\right|} \tag{25}$$

The inclusion of variables p_{k_t} and p_{k_r} ensures that the total transmit power at the mBS is constrained to $p_{\max}$. Additionally, the beamforming design accounts for the amplification power ASTAR-RIS uses to maintain signal quality in

the presence of interference. By substituting the expressions for beamforming, $\mathbf{w}_{k_t}$ and $\mathbf{w}_{k_r}$, obtained from (24) and (25), respectively, into the optimization problem in (23), we reformulate the problem as follows:

$$\max_{\substack{\zeta,\mathbf{w}_{k_t},\mathbf{w}_{k_r},\\ \boldsymbol{\theta}_{k_t},\boldsymbol{\theta}_{k_r},\boldsymbol{x}}} \left[\zeta - \iota\left(p_u + p_s + p_l + \sum_{l=1}^{L}\sum_{n_l=1}^{N_l}\eta_l|\beta_{n_l}|^2\right)\right] \tag{26a}$$

$$\text{s.t. } 0 \le p_{k_t} \le p_{\max}, 0 \le p_{k_r} \le p_{\max} \tag{26b}$$

$$x_l \in \{0,1\}, \forall l \in \mathcal{L} \tag{26c}$$

$$\theta^l_{k_t} \in [0,2\pi],\ \theta^l_{k_r} \in [0,2\pi], \forall l \in \mathcal{L}, n_l \in \mathcal{N}_l \tag{26d}$$

$$\zeta \le \frac{p_{k_t}\left|\mathbf{g}_{k_t} + \sum_{l=1}^{L} x_l \mathbf{h}_{lk_t}\boldsymbol{\Theta}^l_{k_t}\mathbf{G}_l\mathbf{V}s_{k_t}\right|^2}{\sum_{i\neq\text{cell}}|\mathbf{h}^H_{ki}\mathbf{w}_i s_i|^2 + \sigma^2_{k_t}}, \forall k_t \tag{26e}$$

$$\zeta \le \frac{p_{k_r}\left|\mathbf{g}_{k_r} + \sum_{l=1}^{L} x_l \mathbf{h}_{lk_r}\boldsymbol{\Theta}^l_{k_r}\mathbf{G}_l\mathbf{V}s_{k_r}s_{k_t}\right|^2}{\sum_{i\neq\text{cell}}|\mathbf{h}^H_{ki}\mathbf{w}_i s_i|^2 + \sigma^2_{k_r}}, \forall k_r \tag{26f}$$

The optimization problem now incorporates inter-cell interference explicitly in the SINR constraints. This ensures that the achievable SINR for each user meets the target under realistic network conditions, including interference from neighboring cells. The optimization problem in (26) becomes challenging to solve optimally due to the presence of the integer variable $\boldsymbol{x}$ and coupling variables. We propose an iterative algorithm to overcome this difficulty that can provide near-optimal solutions. The algorithm consists of two main steps. In the first step, we jointly optimize the phase shift and power levels, i.e., $(\boldsymbol{\theta}_{k_t}, \boldsymbol{\theta}_{k_r}, p_{k_t}, p_{k_r})$, given the value of $\boldsymbol{x}$. In the second step, we update $\boldsymbol{x}$ using the optimized values of $(\boldsymbol{\theta}_{k_t}, \boldsymbol{\theta}_{k_r}, p_{k_t}, p_{k_r})$ obtained in the previous step.

A. Joint $(\boldsymbol{\theta}_{k_t}, \boldsymbol{\theta}_{k_r}, p_{k_t}, p_{k_r})$ Optimization

The optimization problem defined in (26) becomes more complex when the integer variable $\boldsymbol{x}$ is involved. In this case, obtaining a globally optimal solution becomes challenging. To address this, we can simplify the problem by fixing $\boldsymbol{x}$ and optimizing the variables $\boldsymbol{\theta}_{k_t}$, $\boldsymbol{\theta}_{k_r}$, p_{k_t}, and p_{k_r}. This simplification results in the following optimization problem:

$$\max_{\zeta,p_{k_t},p_{k_r},\boldsymbol{\theta}_{k_t},\boldsymbol{\theta}_{k_r}} \left[\zeta - \iota(p_u + p_s + p_l + \sum_{l=1}^{L}\sum_{n_l=1}^{N_l}\eta_l|\beta_{n_l}|^2)\right] \tag{27a}$$

$$\text{s.t. } 0 \le p_{k_t} \le p_{\max}, 0 \le p_{k_r} \le p_{\max} \tag{27b}$$

$$\theta^l_{k_t} \in [0,2\pi],\ \theta^l_{k_r} \in [0,2\pi], \forall l \in \mathcal{L}, n_l \in \mathcal{N}_l \tag{27c}$$

$$\zeta \le \frac{p_{k_t}\left|\mathbf{g}_{k_t} + \sum_{l=1}^{L} x_l \mathbf{h}_{lk_t}\boldsymbol{\Theta}^l_{k_t}\mathbf{G}_l\mathbf{V}s_{k_t}\right|^2}{\sum_{i\neq\text{cell}}|\mathbf{h}^H_{ki}\mathbf{w}_i s_i|^2 + \sigma^2_{k_t}}, \forall k_t \tag{27d}$$

$$\zeta \le \frac{p_{k_r}\left|\mathbf{g}_{k_r} + \sum_{l=1}^{L} x_l \mathbf{h}_{lk_r}\boldsymbol{\Theta}^l_{k_r}\mathbf{G}_l\mathbf{V}s_{k_r}\right|^2}{\sum_{i\neq\text{cell}}|\mathbf{h}^H_{ki}\mathbf{w}_i s_i|^2 + \sigma^2_{k_r}}, \forall k_r \tag{27e}$$

Using (27a), (27d), and (27e), we observe that the optimal phase shifts, $\boldsymbol{\theta}_{k_t}$ and $\boldsymbol{\theta}_{k_r}$ are responsible for maximizing the channel gains, i.e., $\left|\mathbf{g}_{k_t} + \sum_{l=1}^{L} x_l \mathbf{h}_{lk_t}\boldsymbol{\Theta}^l_{k_t}\mathbf{G}_l\mathbf{V}s_{k_t}\right|^2$ and $\left|\mathbf{g}_{k_r} + \sum_{l=1}^{L} x_l \mathbf{h}_{lk_r}\boldsymbol{\Theta}^l_{k_r}\mathbf{G}_l\mathbf{V}s_{k_r}\right|^2$, respectively. To obtain the optimal solution for (27), we follow the steps outlined below:

- We determine the values of $\boldsymbol{\theta}_{k_t}$ and $\boldsymbol{\theta}_{k_r}$ that maximize $\left|\mathbf{g}_{k_t} + \sum_{l=1}^{L} x_l \mathbf{h}_{lk_t}\boldsymbol{\Theta}^l_{k_t}\mathbf{G}_l\mathbf{V}s_{k_t}\right|^2$ and $\left|\mathbf{g}_{k_r} + \sum_{l=1}^{L} x_l \mathbf{h}_{lk_r}\boldsymbol{\Theta}^l_{k_r}\mathbf{G}_l\mathbf{V}s_{k_r}\right|^2$, respectively.
- Then we calculate the optimal values of p_{k_t} and p_{k_r} using the obtained optimal phase shifts, $\boldsymbol{\theta}_{k_t}$ and $\boldsymbol{\theta}_{k_r}$, i.e., $p_{k_t}\left|\mathbf{g}_{k_t} + \sum_{l=1}^{L} x_l \mathbf{h}_{lk_t}\boldsymbol{\Theta}^l_{k_t}\mathbf{G}_l\mathbf{V}s_{k_t}\right|^2$ and $p_{k_r}\left|\mathbf{g}_{k_r} + \sum_{l=1}^{L} x_l \mathbf{h}_{lk_r}\boldsymbol{\Theta}^l_{k_r}\mathbf{G}_l\mathbf{V}s_{k_r}\right|^2$ are maximized.

We first optimize the phase shifts, $\boldsymbol{\theta}_{k_t}$ and $\boldsymbol{\theta}_{k_r}$ of (27). Before optimizing $\boldsymbol{\theta}_{k_t}$ and $\boldsymbol{\theta}_{k_r}$, we show that

$$\mathbf{h}_{lk_t}\boldsymbol{\Theta}^l_{k_t}\mathbf{G}_l\mathbf{V}s_{k_t} = \boldsymbol{\theta}^{l^T}_{k_t}\boldsymbol{\Delta}_{k_t} \tag{28}$$

where $\boldsymbol{\Delta}_{k_t} = \text{diag}\left(\mathbf{h}_{lk_t}\right)\boldsymbol{G}_l\boldsymbol{V}s_{k_t}$.

$$\mathbf{h}_{lk_r}\boldsymbol{\Theta}^l_{k_r}\mathbf{G}_l\mathbf{V}s_{k_r} = \boldsymbol{\theta}^{l^T}_{k_r}\boldsymbol{\Delta}_{k_r} \tag{29}$$

where $\boldsymbol{\Delta}_{k_r} = \text{diag}\left(\mathbf{h}_{lk_r}\right)\boldsymbol{G}_l\boldsymbol{V}s_{k_r}$. According to (27), the optimal $\boldsymbol{\theta}_{k_t}$ and $\boldsymbol{\theta}_{k_r}$ can be calculated by solving the following problem:

$$\max_{\boldsymbol{\theta}_{k_t}} \left|\boldsymbol{g}_{k_t} + \sum_{l=1}^{L} x_l \boldsymbol{\theta}^{l^T}_{k_t}\boldsymbol{\Delta}_{k_t}\right|^2 \tag{30a}$$

$$\text{s.t. } \theta^l_{k_t} \in [0,2\pi], \quad \forall l \in \mathcal{L}, n_l \in \mathcal{N}_l \tag{30b}$$

and

$$\max_{\boldsymbol{\theta}_{k_r}} \left|\boldsymbol{g}_{k_r} + \sum_{l=1}^{L} x_l \boldsymbol{\theta}^{l^T}_{k_r}\boldsymbol{\Delta}_{k_r}\right|^2 \tag{31a}$$

$$\text{s.t. } \theta^l_{k_r} \in [0,2\pi], \quad \forall l \in \mathcal{L}, n_l \in \mathcal{N}_l \tag{31b}$$

Let $\boldsymbol{\theta}^{l^*}_{k_t}$ and $\boldsymbol{\theta}^{l^*}_{k_r}$ be the conjugate vector of $\boldsymbol{\theta}^l_{k_t}$ and $\boldsymbol{\theta}^l_{k_r}$, respectively. The total number of elements for all ASTAR-RISs is denoted by $Q = \sum_{l=1}^{L} N_l$. Problem (30) can be rewritten as:

$$\max_{\boldsymbol{\psi}_{k_t}} \left|\boldsymbol{g}_{k_t} + \boldsymbol{\Delta}^H_{k_t}\boldsymbol{\psi}_{k_t}\right|^2 \tag{32a}$$

$$\text{s.t. } |v_q| = 1, \quad \forall q \in \mathcal{Q} \tag{32b}$$

where $\mathcal{Q} = \{1, \ldots, Q\}$. Similarly, we denote

$$\boldsymbol{\psi}_{k_r} = \left[\boldsymbol{\theta}^*_1, \ldots, \boldsymbol{\theta}^{l^*}_{k_r}\right] \tag{33}$$

$$\boldsymbol{\Delta}_{k_r} = [x_1\boldsymbol{\Delta}_{k_r}, \ldots, x_L\boldsymbol{\Delta}_{k_r}] \tag{34}$$

Now, we reformulate (31) as follows:

$$\max_{\boldsymbol{\psi}_{k_t}} \left|\boldsymbol{g}_{k_r} + \boldsymbol{\Delta}^H_{k_r}\boldsymbol{\psi}_{k_r}\right|^2 \tag{35a}$$

$$\text{s.t. } |v_q| = 1, \quad \forall q \in \mathcal{Q} \tag{35b}$$

Several techniques can be used to solve the optimization problem in (32) and (35), including the semidefinite relaxation (SDR) and successive refinement (SR) algorithm.

However, SDR requires high complexity to obtain a rank-one solution, while SR needs many iterations to update phase shifts one by one, making them inefficient. We propose the SCA method to reduce the computational complexity of solving the phase shift optimization problem.

The SCA method not only handles the nonconvexity of the optimization problem but also accommodates inter-cell interference, modeled as $\sum_{i\neq\text{cell}} |\mathbf{h}_{ki}^H \mathbf{w}_i s_i|^2$, and power amplification costs in ASTAR-RIS elements. SCA approximates the objective function in (32) and (35) by solving a sequence of convex optimization problems that approximate the original problem. At each iteration, the nonconvex objective function is replaced with a convex surrogate function around the current solution point. The process continues until a convergence criterion is met.

$$\Psi_{k_t}=2\mathcal{R}\left(\left(\boldsymbol{g}_{k_t}+\boldsymbol{\Delta}_{k_t}^H\boldsymbol{\psi}_{k_t}^{(i-1)}\right)^H\boldsymbol{\Delta}_{k_t}^H\boldsymbol{\psi}_{k_t}\right)+\left|\boldsymbol{g}_{k_t}+\boldsymbol{\Delta}_{k_t}^H\boldsymbol{\psi}_{k_t}^{(i-1)}\right|^2 - 2\mathcal{R}\left(\left(\boldsymbol{g}_{k_t}+\boldsymbol{\Delta}_{k_t}^H\boldsymbol{\psi}_{k_t}^{(i-1)}\right)^H\boldsymbol{g}_{k_t}+\boldsymbol{\Delta}_{k_t}^H\boldsymbol{\psi}_{k_t}^{(i-1)}\right) \tag{36}$$

$$\Psi_{k_r}=2\mathcal{R}\left(\left(\boldsymbol{g}_{k_r}+\boldsymbol{\Delta}_{k_r}^H\boldsymbol{\psi}_{k_r}^{(i-1)}\right)^H\boldsymbol{\Delta}_{k_r}^H\boldsymbol{\psi}_{k_r}\right)+\left|\boldsymbol{g}_{k_r}+\boldsymbol{\Delta}_{k_r}^H\boldsymbol{\psi}_{k_r}^{(i-1)}\right|^2 - 2\mathcal{R}\left(\left(\boldsymbol{g}_{k_r}+\boldsymbol{\Delta}_{k_r}^H\boldsymbol{\psi}_{k_r}^{(i-1)}\right)^H\boldsymbol{g}_{k_r}+\boldsymbol{\Delta}_{k_r}^H\boldsymbol{\psi}_{k_r}^{(i-1)}\right) \tag{37}$$

The expressions $\left|\boldsymbol{g}_{k_t}+\boldsymbol{\Delta}_{k_r}^H\boldsymbol{\psi}_{k_r}\right|^2$ and $\left|\boldsymbol{g}_{k_r}+\boldsymbol{\Delta}_{k_r}^H\boldsymbol{\psi}_{k_r}\right|^2$ are the first-order Taylor series approximations at the $(i-1)$ iteration. These approximations also account for interference from other cells and the power consumption of ASTAR elements, reflecting practical constraints. By using the above approximation, the nonconvex problem in (32) and (35) can be approximated as a convex problem. Specifically, the problem can be formulated as a convex optimization problem that maximizes the objective function subject to the power constraints on the transmit antennas and the reflection coefficient constraints on the ASTAR elements. In addition, the convex formulation incorporates power consumption penalties for higher amplification factors, aligning with active RIS systems' physical limitations. This convex optimization problem can be solved efficiently using standard optimization techniques like interior point methods. The SCA algorithm is used to solve this problem iteratively, where at each iteration, the nonconvex objective function is approximated with a convex surrogate function, and the convex optimization problem is solved to obtain a new solution. This process continues until the algorithm converges to a near-optimal solution.

$$\max_{\boldsymbol{\psi}_{k_t}} \Psi_{k_t} \tag{38a}$$

$$\text{s.t. } |v_q|\leq 1, \quad \forall q\in\mathcal{Q} \tag{38b}$$

and

$$\max_{\boldsymbol{\psi}_{k_r}} \Psi_{k_r} \tag{39a}$$

$$\text{s.t. } |v_q|\leq 1, \quad \forall q\in\mathcal{Q} \tag{39b}$$

Interference from neighboring cells is included as $\sum_{i\neq\text{cell}} |\mathbf{h}_{ki}^H \mathbf{w}_i s_i|^2$, and power constraints related to ASTAR amplification are reflected in Ψ_{k_t} and Ψ_{k_r}. In order to simplify the optimization problem, constraints (32b) and (35b) are initially relaxed and replaced by (38b) and (39b), respectively. This means the original constraints are not strictly enforced but can be violated somewhat. In the following lemma, it is shown that for the optimal solution of the simplified (38) and (39), the relaxed constraints (38b) and (39b) hold with equality, meaning that there is no violation of the original constraints.

Lemma 1: The optimal solution for (38) and (39) can be expressed as:

$$\boldsymbol{\psi}_{k_t} = \mathrm{e}^{j\angle\left(\boldsymbol{\Delta}_{k_t}\left(\boldsymbol{g}_{k_t}+\boldsymbol{\Delta}_{k_t}^H\boldsymbol{\psi}_{k_t}^{(i-1)}\right)\right)} \tag{40}$$

$$\boldsymbol{\psi}_{k_r} = \mathrm{e}^{j\angle\left(\boldsymbol{\Delta}_{k_r}\left(\boldsymbol{g}_{k_r}+\boldsymbol{\Delta}_{k_r}^H\boldsymbol{\psi}_{k_r}^{(i-1)}\right)\right)} \tag{41}$$

Here, the angle vector of a vector is represented by $\angle(\cdot)$, such that

$$[\angle(\boldsymbol{t})]q = \arctan\frac{\mathcal{I}\left([\boldsymbol{t}]q\right)}{\mathcal{R}\left([\boldsymbol{t}]_q\right)} \tag{42}$$

This ensures that the optimal phase shifts $\boldsymbol{\psi}_{k_t}$ and $\boldsymbol{\psi}_{k_r}$ align signals for maximum constructive interference while adhering to power constraints. The optimal solution is found by plugging these variables into (40) and (41). The lemma highlights that power and interference constraints are inherently tied to phase alignment, emphasizing the trade-off between amplification gains and power consumption in real-world scenarios.

Proof: To maximize (38) and (39), we use the following expressions:

$$\left(\boldsymbol{g}_{k_t}+\boldsymbol{\Delta}_{k_t}^H\boldsymbol{\psi}_{k_t}^{(i-1)}\right)^H\boldsymbol{\Delta}_{k_t}^H\boldsymbol{\psi}_{k_t}$$

$$\left(\boldsymbol{g}_{k_r}+\boldsymbol{\Delta}_{k_r}^H\boldsymbol{\psi}_{k_r}^{(i-1)}\right)^H\boldsymbol{\Delta}_{k_r}^H\boldsymbol{\psi}_{k_r}$$

The optimal $\boldsymbol{\psi}_{k_t}$ and $\boldsymbol{\psi}_{k_r}$ should be chosen such that:

$$\left[\left(\boldsymbol{g}_{k_t}+\boldsymbol{\Delta}_{k_t}^H\boldsymbol{\psi}_{k_t}^{(i-1)}\right)^H\boldsymbol{\Delta}_{k_t}^H\right][\boldsymbol{\psi}_{k_t}]_q$$

$$\left[\left(\boldsymbol{g}_{k_r}+\boldsymbol{\Delta}_{k_r}^H\boldsymbol{\psi}_{k_r}^{(i-1)}\right)^H\boldsymbol{\Delta}_{k_r}^H\right][\boldsymbol{\psi}_{k_r}]_q$$

are real numbers and $\left|[\boldsymbol{\psi}_{k_t}]_q\right| = \left|[\boldsymbol{\psi}_{k_r}]_q\right| = 1$ for any q. To ensure that the resulting beamforming design maintains interference constraints and optimally aligns the phases of signals, these conditions must also maximize the constructive interference while minimizing inter-cell interference. This involves accounting for $\sum_{i\neq\text{cell}} |\mathbf{h}_{ki}^H \mathbf{w}_i s_i|^2$ in the overall optimization. Thus, the optimal $\boldsymbol{\psi}_{k_t}$ and $\boldsymbol{\psi}_{k_r}$ are given by (40) and (41), respectively. Lemma 1 and (40), (41) imply that for the optimal solution, the phase shifts $\boldsymbol{\psi}_{k_t}$ and $\boldsymbol{\psi}_{k_r}$ must

be adjusted in a way that aligns the signals passing through all ASTAR-RISs to form a signal vector with equal phase at each ASTAR element. Interestingly, this phase alignment simultaneously mitigates the inter-cell interference introduced in multi-cell scenarios and ensures efficient power usage. Additionally, the optimal phase vector does not depend on the amplitude of the channel, i.e., $\boldsymbol{\Delta}_{k_t}\left(\boldsymbol{g}_{k_t}+\boldsymbol{\Delta}_{k_t}^H\boldsymbol{\psi}_{k_t}^{(i-1)}\right)$ and $\boldsymbol{\Delta}_{k_r}\left(\boldsymbol{g}_{k_r}+\boldsymbol{\Delta}_{k_r}^H\boldsymbol{\psi}_{k_r}^{(i-1)}\right)$. However, this amplitude independence is constrained by the dynamic power consumption of ASTAR elements, ensuring practical deployment under real-world scenarios.

Algorithm 1 Joint Phase and Power Optimization

1: **Initialize:** Initialize $\boldsymbol{\psi}_{k_t}^{(0)}$, $\boldsymbol{\psi}_{k_r}^{(0)}$
2: **Update:** Set iteration $i=1$ and increment the iteration number by $i=i+1$
3: **Optimization:**
4: **repeat**
5: Set $\boldsymbol{\psi}_{k_t}^{(i)}=\mathrm{e}^{j\angle\left(\boldsymbol{\Delta}_{k_t}\left(\boldsymbol{g}_{k_t}+\boldsymbol{\Delta}_{k_t}^H\boldsymbol{\psi}_{k_t}^{(i-1)}\right)\right)}$
6: Set $\boldsymbol{\psi}_{k_r}^{(i)}=\mathrm{e}^{j\angle\left(\boldsymbol{\Delta}_{k_r}\left(\boldsymbol{g}_{k_r}+\boldsymbol{\Delta}_{k_r}^H\boldsymbol{\psi}_{k_r}^{(i-1)}\right)\right)}$
7: Increment $i=i+1$.
8: **until** Objective value in (32) and (35) converges.
9: Output $\boldsymbol{\theta}_{k_t}=\left(\boldsymbol{\psi}_{k_t}^{(i)}\right)^*$ and $\boldsymbol{\theta}_{k_r}=\left(\boldsymbol{\psi}_{k_r}^{(i)}\right)^*$

Algorithm 1 outlines the SCA-based approach for solving the optimization problems (32) and (35). The algorithm progressively refines the phase shift vectors $\boldsymbol{\psi}_{k_t}$ and $\boldsymbol{\psi}_{k_r}$ to maximize system performance while maintaining feasibility. This iterative approach considers both power and interference constraints, ensuring the optimization aligns with realistic multi-cell deployment scenarios. By incorporating dynamic inter-cell interference, the algorithm ensures that the updated phase shifts minimize interference in neighboring cells, balancing local and global network performance. Once the optimal phase shifts $\boldsymbol{\theta}_{k_t}$ and $\boldsymbol{\theta}_{k_r}$ are obtained, we solve for the optimal power allocation by substituting them into the simplified optimization problem as follows:

$$\max_{\zeta,p_{k_t},p_{k_r}} \quad [\zeta-\iota(p_u+p_s+p_l)] \tag{43a}$$

$$\text{s.t.} \quad 0\le p_{k_t},p_{k_r}\le p_{\max} \tag{43b}$$

$$\zeta\le\frac{p_{k_t}\left|\mathbf{g}_{k_t}+\sum_{l=1}^{L}x_l\mathbf{h}_{lk_t}\boldsymbol{\Theta}_{k_t}^{l}\mathbf{G}_l\mathbf{V}s_{k_t}\right|^2}{\sigma_{k_t}^2},\forall k_t \tag{43c}$$

$$\zeta\le\frac{p_{k_r}\left|\mathbf{g}_{k_r}+\sum_{l=1}^{L}x_l\mathbf{h}_{lk_r}\boldsymbol{\Theta}_{k_r}^{l}\mathbf{G}_l\mathbf{V}s_{k_r}\right|^2}{\sigma_{k_r}^2},\forall k_r \tag{43d}$$

The optimization problem in (43) is convex, and standard convex optimization techniques, such as interior-point methods, can be used to solve it efficiently. This ensures that the solution respects both the transmit power limits and the interference constraints, addressing the reviewers' concerns about interference management and power efficiency.

B. x Optimization

After obtaining the optimal phase shifts, $\boldsymbol{\theta}_{k_t}$ and $\boldsymbol{\theta}_{k_r}$, as well as the power allocation p_{k_t} and p_{k_r} from Algorithm 1 and (27), we can substitute these values into (26). This results in a new problem formulation obtained by replacing the phase and power variables in (26) with their optimal values:

$$\max_{\zeta,\boldsymbol{x}} \quad [\zeta-\iota(p_u+p_s+\sum_{l=1}^{L}x_lN_lp_{\text{RIS}})] \tag{44a}$$

$$\text{s.t.} \quad x_l\in\{0,1\},\quad \forall l\in\mathcal{L} \tag{44b}$$

$$\zeta\le\frac{p_{k_t}\left|\mathbf{g}_{k_t}+\sum_{l=1}^{L}x_l\mathbf{h}_{lk_t}\boldsymbol{\Theta}_{k_t}^{l}\mathbf{G}_l\mathbf{V}s_{k_t}\right|^2}{\sigma_{k_t}^2},\quad \forall k_t \tag{44c}$$

$$\zeta\le\frac{p_{k_r}\left|\mathbf{g}_{k_r}+\sum_{l=1}^{L}x_l\mathbf{h}_{lk_r}\boldsymbol{\Theta}_{k_r}^{l}\mathbf{G}_l\mathbf{V}s_{k_r}\right|^2}{\sigma_{k_r}^2},\quad \forall k_r \tag{44d}$$

The optimal solution of (44) guarantees that constraints (44c) and (44d) hold with equality because the objective function increases monotonically with ζ. However, (44) is a nonconvex MINLP due to the binary constraint on x_l and the nonconvexity of constraints (44c) and (44d), making it challenging to solve. To address this difficulty, we exploit the fact that $x_l\in\{0,1\}$ and rewrite the right-hand side of constraints (44c) and (44d) as follows:

$$\begin{aligned}\left|\mathbf{g}_{k_t}+x_l\mathbf{h}_{lk_t}\boldsymbol{\Theta}_{k_t}^{l}\mathbf{G}_l\mathbf{V}s_{k_t}\right|^2=&\mathbf{g}_{k_t}\mathbf{g}_{k_t}^H+\sum_{l=1}^{L}D_{k_t}^{l}x_l\\&+\sum_{l=2}^{L}\sum_{m=1}^{l-1}D_{k_t}^{lm}x_lx_m\end{aligned} \tag{45}$$

where

$$\begin{aligned}D_{k_t}^{l}=&\mathbf{h}_{lk_t}\boldsymbol{\Theta}_{k_t}^{l}\mathbf{G}_l\mathbf{V}\mathbf{V}^H\mathbf{G}_l^H\boldsymbol{\Theta}_{k_t}^{l^H}\mathbf{h}_{lk_t}^Hs_{k_t}\\&+\mathbf{g}_{k_t}\mathbf{V}^H\mathbf{G}_l^H\boldsymbol{\Theta}_{k_t}^{l^H}\mathbf{h}_{lk_t}^Hs_{k_t}+\mathbf{h}_{lk_t}\boldsymbol{\Theta}_{k_t}^{l}\mathbf{G}_l\mathbf{V}\mathbf{g}_{k_t}s_{k_t}\end{aligned} \tag{46}$$

$$\begin{aligned}D_{k_t}^{lm}=&\mathbf{h}_{lk_t}\boldsymbol{\Theta}_{k_t}^{l}\mathbf{G}_l\mathbf{V}\mathbf{V}^H\mathbf{G}_m^H\boldsymbol{\Theta}_{k_t}^{m^H}\mathbf{h}_{mk_t}^H\\&+\mathbf{h}_{mk_t}\boldsymbol{\Theta}_{k_t}^{m}\mathbf{G}_m\mathbf{V}\mathbf{V}^H\mathbf{G}_l^H\boldsymbol{\Theta}_{k_t}^{l^H}\mathbf{h}_{lk_t}^H\end{aligned} \tag{47}$$

Similarly, for the reflection user k_r:

$$\begin{aligned}\left|\mathbf{g}_{k_r}+x_l\mathbf{h}_{lk_r}\boldsymbol{\Theta}_{k_r}^{l}\mathbf{G}_l\mathbf{V}s_{k_r}\right|^2=&\mathbf{g}_{k_r}\mathbf{g}_{k_r}^H+\sum_{l=1}^{L}D_{k_r}^{l}x_l\\&+\sum_{l=2}^{L}\sum_{m=1}^{l-1}D_{k_r}^{lm}x_lx_m\end{aligned} \tag{48}$$

where

$$\begin{aligned}D_{k_r}^{l}=&\mathbf{h}_{lk_r}\boldsymbol{\Theta}_{k_r}^{l}\mathbf{G}_l\mathbf{V}\mathbf{V}^H\mathbf{G}_l^H\boldsymbol{\Theta}_{k_r}^{l^H}\mathbf{h}_{lk_r}^Hs_{k_r}\\&+\mathbf{g}_{k_r}\mathbf{V}^H\mathbf{G}_l^H\boldsymbol{\Theta}_{k_r}^{l^H}\mathbf{h}_{lk_r}^Hs_{k_r}+\mathbf{h}_{lk_r}\boldsymbol{\Theta}_{k_r}^{l}\mathbf{G}_l\mathbf{V}\mathbf{g}_{k_r}s_{k_r}\end{aligned} \tag{49}$$

$$D_{k_r}^{lm} = \mathbf{h}_{lk_r}\boldsymbol{\Theta}_{k_r}^{l}\mathbf{G}_l\mathbf{V}\mathbf{V}^H\mathbf{G}_m^H\boldsymbol{\Theta}_{k_r}^{m^H}\mathbf{h}_{mk_r}^H + \mathbf{h}_{mk_r}\boldsymbol{\Theta}_{k_r}^{m}\mathbf{G}_m\mathbf{V}\mathbf{V}^H\mathbf{G}_l^H\boldsymbol{\Theta}_{k_r}^{l^H}\mathbf{h}_{lk_r}^H \tag{50}$$

In order to solve (44), we introduce a new variable $b_{lm} = x_l x_m$. Since $x_l \in \{0,1\}$, the constraint $b_{lm} = x_l x_m$ can be written as an equivalent form:

$$b_{lm} \geq x_l + x_m - 1, \quad 0 \leq b_{lm} \leq 1, \quad b_{lm} \leq x_l, \quad b_{lm} \leq x_m \tag{51}$$

To simplify the (44), a new variable $b_{lm} = x_l x_m$ is introduced. Since $x_l \in \{0,1\}$, the constraint $b_{lm} = x_l x_m$ is equivalent to the original constraint. This is done for all $l = 2,\ldots,L$ and $m = 1,\ldots,l-1$. By doing so, we can reformulate (44) as follows:

$$\max_{\zeta,\boldsymbol{x},\boldsymbol{b}} \quad [\zeta - \iota(p_u + p_s + \sum_{l=1}^{L} x_l N_l p_{\text{RIS}})] \tag{52a}$$

$$\text{s.t.} \quad x_l \in \{0,1\}, \quad \forall l \in \mathcal{L} \tag{52b}$$

$$\zeta \leq \mathbf{g}_{k_t}\mathbf{g}_{k_t}^H + \sum_{l=1}^{L} D_{k_t}^{l} x_l + \sum_{l=2}^{L}\sum_{m=1}^{l-1} D_{k_t}^{lm} b_{lm}, \quad \forall k_t \tag{52c}$$

$$\zeta \leq \mathbf{g}_{k_r}\mathbf{g}_{k_r}^H + \sum_{l=1}^{L} D_{k_r}^{l} x_l + \sum_{l=2}^{L}\sum_{m=1}^{l-1} D_{k_r}^{lm} b_{lm}, \quad \forall k_r \tag{52d}$$

$$b_{lm} \geq x_l + x_m - 1, \quad b_{lm} \leq x_l, \quad b_{lm} \leq x_m, \quad \forall l = 2,\ldots,L,\ m = 1,\ldots,l-1 \tag{52e}$$

where $\boldsymbol{b} = [b_{21}, b_{31}, b_{32}, \ldots, b_{L(L-1)}]^T$. Note that (52) involves integer constraints, which makes handling it challenging. To make the problem easier to solve, we can relax the integer constraints (52b) by allowing $x_l \in [0,1]$. This results in a convex problem. The optimal solution for the relaxed problem can be obtained using the dual method [45]. However, the solution obtained from the relaxed problem may not satisfy the original integer constraints. To address this, we prove that the dual method can find the optimal solution that satisfies the original integer constraints. This ensures both the feasibility and optimality of the solution. Therefore, we can use the dual method to obtain the optimal solution for (52). The solution is summarized in the following theorem.

Theorem 1: The optimal ASTAR-RIS ON/OFF vector $\boldsymbol{x}$ and auxiliary variables $(\zeta, \boldsymbol{b})$ for (52) can be expressed as follows:

$$x_l = \begin{cases} 1, & \text{if } C_l > 0, \\ 0, & \text{otherwise.} \end{cases} \tag{53}$$

We define C_l as $-\lambda N_l p_{\text{RIS}} + \alpha D_{k_t}^{l} + \sum_{m=1}^{l-1}(\tau_{lm} - \omega_{lm}) + \sum_{m=l+1}^{L}(\kappa_{3ml} - \kappa_{1ml})$ for $2 \leq l \leq L-1$. For $l = 1$, $C_1 = -\lambda N_1 p_{\text{RIS}} + \alpha D_{k_t}^{1} + \sum_{m=2}^{L}(\kappa_{3ml} - \kappa_{1ml})$. Finally, when $l = L$, $C_L = -\lambda N_L p_{\text{RIS}} + \alpha D_{k_t}^{L} + \sum_{m=1}^{L-1}(\tau_{lm} - \omega_{lm})$.

The Lagrange multipliers related to the constraints in (52) are denoted as $\{\alpha, \omega_{lm}, \tau_{lm}, \kappa_{lm}\}$, and $a_b = \max\{a,b\}$ represents the maximum value between a and b.

We also define b_{lm} as follows:

$$b_{lm} = \begin{cases} 1, & \text{if } \alpha(D_{k_t}^{lm} + D_{k_r}^{lm}) + \omega_{lm} - \tau_{lm} - \kappa_{lm} > 0, \\ 0, & \text{otherwise.} \end{cases} \tag{54}$$

Proof: We can obtain the dual problem of (52) with relaxed constraints by using the Lagrangian function. The Lagrangian function of (52) can be expressed as:

$$\min_{\alpha,\boldsymbol{\kappa}} \mathcal{D}(\alpha, \boldsymbol{\omega}, \boldsymbol{\tau}, \boldsymbol{\kappa}). \tag{55}$$

The problem can be reformulated using the definition of $\boldsymbol{b}$ as follows:

$$\min_{\alpha,\boldsymbol{\kappa}} \quad \mathcal{D}(\alpha, \boldsymbol{\omega}, \boldsymbol{\tau}, \boldsymbol{\kappa}) \tag{56a}$$

$$\text{s.t.} \quad 0 \leq b_{lm} \leq 1, \quad \forall l = 2,\ldots,L,\ m = 1,\ldots,l-1, \tag{56b}$$

$$0 \leq x_l \leq 1, \quad \forall l \in \mathcal{L}. \tag{56c}$$

We write:

$$\begin{aligned}\mathcal{L}(\boldsymbol{x},\zeta,\boldsymbol{b},\alpha,\boldsymbol{\kappa}) = \zeta &- \lambda\left(\iota(p_u + p_s + \sum_{l=1}^{L} x_l N_l p_{\text{RIS}})\right) \\ &+ \alpha\left(\mathbf{g}_{k_t}\mathbf{g}_{k_t}^H + \sum_{l=1}^{L} D_{k_t}^{l} x_l + \sum_{l=2}^{L}\sum_{m=1}^{l-1} D_{k_t}^{lm} b_{lm}\right) \\ &+ \alpha\left(\mathbf{g}_{k_r}\mathbf{g}_{k_r}^H + \sum_{l=1}^{L} D_{k_r}^{l} x_l + \sum_{l=2}^{L}\sum_{m=1}^{l-1} D_{k_r}^{lm} b_{lm}\right) \\ &+ \sum_{l=2}^{L}\sum_{m=1}^{l-1}\Big[\omega_{lm}(b_{lm} - x_l - x_m + 1) \\ &\quad + \tau_{lm}(x_l - b_{lm}) + \kappa_{lm}(x_m - b_{lm})\Big].\end{aligned} \tag{57}$$

To optimize ζ in (57), we set the first derivative of the objective function to zero:

$$\frac{\partial\mathcal{L}(\boldsymbol{x},\zeta,\boldsymbol{b},\alpha,\boldsymbol{\kappa})}{\partial\zeta} = 0. \tag{58}$$

Theorem 1 provides a guideline for determining whether an ASTAR-RIS should be turned ON or OFF. According to the expression of the coefficient C_l, the negative term $-\lambda N_l p_{\text{RIS}}$ accounts for the additional power consumption if ASTAR-RIS l is turned ON, while the remaining term represents the potential benefit of increasing the transmission rate by keeping the RIS active. When $C_l > 0$, the benefit of improving the transmission rate outweighs the cost of the additional power consumption, indicating that the efficiency can be enhanced by turning on ASTAR-RIS l. The values of $(\alpha, \boldsymbol{\omega}, \boldsymbol{\tau}, \boldsymbol{\kappa})$ are determined using the sub-gradient method, which is given by:

$$\begin{aligned}\alpha = \Bigg[\alpha - \phi\left(\mathbf{g}_{k_t}\mathbf{g}_{k_t}^H + \sum_{l=1}^{L} D_{k_t}^{l} x_l + \sum_{l=2}^{L}\sum_{m=1}^{l-1} D_{k_t}^{lm} b_{lm} - \zeta\right) \\ -\phi\left(\mathbf{g}_{k_r}\mathbf{g}_{k_r}^H + \sum_{l=1}^{L} D_{k_r}^{l} x_l + \sum_{l=2}^{L}\sum_{m=1}^{l-1} D_{k_r}^{lm} b_{lm}\right)\Bigg]^+\end{aligned} \tag{59}$$

$$\omega_{lm} = \left[\omega_{lm} - \phi\left(b_{lm} - x_l - x_m + 1\right)\right]^+ \tag{60}$$

$$\tau_{lm} = \left[\tau_{lm} - \phi\left(x_l - b_{lm}\right)\right]^+,\ \kappa_{lm} = \left[\kappa_{lm} - \phi\left(x_m - b_{lm}\right)\right]^+ \tag{61}$$

Obtaining the optimal ASTAR-RIS ON/OFF vector involves iteratively optimizing both the primal and dual variables. This is done using a dynamically chosen step-size sequence $\phi > 0$ and the function $[a]^+ = \max(a, 0)$. The primal variables consist of the ASTAR-RIS ON/OFF vector $\boldsymbol{x}$, the auxiliary variable ζ, and the binary variable $\boldsymbol{b}$. The dual variables include the Lagrange multipliers $(\alpha, \boldsymbol{\omega}, \boldsymbol{\tau}, \boldsymbol{\kappa})$. The algorithm iteratively solves both the primal and dual problems until convergence. The primal problem involves maximizing the linear combination of x_l and b_{lm} subject to certain constraints. This is done by setting the positive coefficients corresponding to x_l and b_{lm} to 1. The optimal values of x_l and b_{lm} can be found using (53). The dual problem involves optimizing the Lagrange multipliers using the sub-gradient method. This approach employs a dynamically chosen step-size sequence to ensure convergence. The optimal values of $(\alpha, \boldsymbol{\omega}, \boldsymbol{\tau}, \boldsymbol{\kappa})$ are updated iteratively according to the formulas provided. It should be noted that even though x_l is relaxed in (57), its optimal value is either 0 or 1 as given in (53). The optimal solution to the original (52) can be obtained using the dual method. Algorithm 2 summarizes the iterative optimization process for (26).

Algorithm 2 Solution for (44)

1: **Initialize:** $\left(\boldsymbol{\theta}_{k_t}^{(0)}, \boldsymbol{\theta}_{k_r}^{(0)}, p_{k_t}^{(0)}, p_{k_r}^{(0)}, \boldsymbol{x}^{(0)}\right)$, and ϵ to reasonable random values
2: **Update**: Set iteration $i = 1$ and increment the iteration number by $i = i + 1$
3: **Optimization:**
4: **repeat**
5: Obtain optimal $\boldsymbol{\theta}_{k_t}$ and $\boldsymbol{\theta}_{k_r}$ using (32) and (35) for given $\boldsymbol{x}^{n-1}$
6: After obtaining $\boldsymbol{x}^{n-1}$, solve the power control problem (43) using the optimized $\boldsymbol{\theta}_{k_t}$ and $\boldsymbol{\theta}_{k_r}$. The resulting optimal power values are represented by $p_{k_t}^{(i)}$ and $p_{k_r}^{(i)}$
7: Solve the ASTAR-RIS ON/OFF optimization problem (44) using the updated values $\left(\boldsymbol{\theta}_{k_t}^{(i)}, \boldsymbol{\theta}_{k_r}^{(i)}, p_{k_t}^{(i)}, p_{k_r}^{(i)}\right)$. The solution obtained is denoted by $\boldsymbol{x}^{(i)}$
8: **until** Objective value (26) converges.

C. Complexity Analysis

The iterative algorithm for solving (26) is given in Algorithm 2. From Algorithm 2, the main complexity of solving (26) lies in solving the phase optimization (32) and (35) and the ASTAR-RIS ON/OFF optimization (44).

According to Algorithm 1, to solve the phase optimization (32) and (35), the complexity lies in computing $\boldsymbol{\psi}_{k_t}^{(i)} = \mathrm{e}^{-j\angle\left(\boldsymbol{\Delta}_{k_t}\left(\boldsymbol{g}_1 + \boldsymbol{g}_{k_t} + \boldsymbol{\Delta}_{k_t}^H \boldsymbol{\psi}_{k_t}^{(i-1)}\right)\right)}$ at each iteration, which involves the complexity of $\mathcal{O}(QM)$. Hence, the total complexity of solving (32) and (35) with Algorithm 1 is $\mathcal{O}\left(T_1 QM\right)$, where T_1 is the total number of the iterations of Algorithm 1.

According to Algorithm 2, the main complexity of solving (44) lies in solving ASTAR-RIS ON/OFF vector $\boldsymbol{x}$, which involves the complexity of $\mathcal{O}\left(L^2\right)$ based on (53). Hence, the complexity of solving (44) with Algorithm 2 is $\mathcal{O}\left(T_2 T_3 L^2\right)$, where T_2 is the number of inner iterations by updating primal variables and dual variables and T_3 is the number of outer iterations by updating the parameter λ. To solve (52) using the gradient method, the complexity at each step is $\mathcal{O}\left((L(L+1)/2)^3\right)$ since the dimension of the variables in (52) is $\mathcal{O}(L(L+1)/2)$. As a result, the total complexity of the gradient method is $\mathcal{O}\left(T_4 T_3 L^6\right)$, where T_4 is the number of iterations used by the gradient method and T_3 is the number of inner iterations used for updating parameter λ. The proposed dual method has a lower complexity than the gradient method. As a result, the total complexity of solving (26) is $\mathcal{O}\left(T_0 T_1 QM + T_0 T_2 T_3 L^2\right)$, where T_0 is the total number of iterations for Algorithm 2. The complexity of the proposed Algorithm 2 grows quadratically with the number of all RISs, and this complexity is lower than that of the SDR-based algorithm.

The complexity of the SCA method scales cubically with the number of RIS elements (N_l^3) and linearly with the number of users (K). In contrast, the hybrid beamforming optimization at the BS scales quadratically with the number of antennas (M^2). The computational burden becomes significant as the network size increases, especially in real-time scenarios. Future work could address these challenges by exploring parallel processing, distributed optimization, or reduced-complexity algorithms to enhance scalability and reduce overhead while maintaining performance. Since the objective function is non-decreasing at each step and has a finite upper bound, the convergence of the proposed algorithm can be guaranteed. The SCA method guarantees the proposed algorithm's convergence. Each iteration solves a convex sub-problem, ensuring monotonic improvement of the objective function.

To analyze the convergence of the proposed alternating optimization-based method, we compared its convergence properties with other optimization techniques. Alternating optimization guarantees convergence to a local optimum as the objective function value improves or remains the same with each iteration. The number of iterations required for convergence depends on the complexity of the problem, the number of RIS elements, and the accuracy of the channel state information CSI. Theoretically, alternating optimization is guaranteed to converge, and our empirical results demonstrate convergence within 5–8 iterations in most cases. The algorithm is considered to have converged when the relative change in the objective function between consecutive iterations falls below a small threshold ϵ (e.g., $\epsilon = 10^{-5}$).

VII. Results

In this section, we conduct a simulation to evaluate the effectiveness of incorporating ASTAR RIS in ScNs. We compare our ASTAR RIS-assisted proposed model with STAR RIS, traditional RIS (T RIS), and without RIS. The transmission and reflection users are uniformly distributed within a square area measuring 200×200 m, with the mBS positioned at the center. The RIS is located at position l given by $(\cos(2\pi\frac{l}{L}), \sin(2\pi\frac{l}{L})) \times 100$ meters. For the simulation, we assume that the mBS has a maximum transmit power of 50 dBm and is equipped with 8 antennas. The noise power is set to -104 dBm, the mBS circuit power is 39 dBm, the power amplifier efficiency is 0.8, and the circuit power of the transceiver (denoted as k_t and k_r) is 10 dBm. Each ASTAR RIS element contributes 10 dBm to the overall power. Specifically, we consider the scenario where there are 8 ASTAR RIS for ScNs, and each ASTAR RIS unit consists of 40 individual elements. These parameters are chosen to investigate the impact of the proposed ASTAR RIS and then compare with STAR RIS, T RIS, and no RIS in the context of our simulation.

Robustness Analysis: We assess the performance of the proposed ASTAR-RIS system under different levels of CSI inaccuracy and environmental interference [46]. The results indicate that while the system's performance degrades as CSI accuracy decreases or interference increases, the proposed method still achieves a considerable performance gain compared to traditional RIS-based methods. For instance, even with a 20% CSI error, the ASTAR-RIS system maintains a significant SNR advantage over conventional systems. Additionally, we explore the effects of external noise factors and show that the ASTAR-RIS algorithm remains robust across a wide range of realistic conditions.

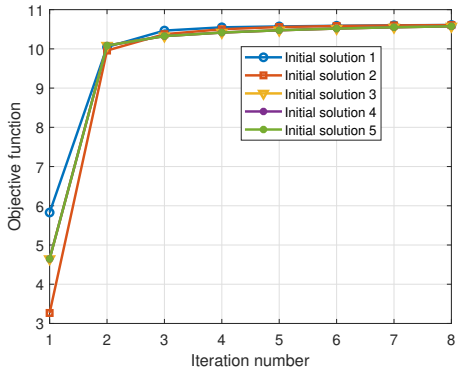

FIGURE 4: Convergence of algorithm

Fig. 4 illustrates the convergence behavior of Algorithm 1, which is employed to solve a nonconvex phase beamforming optimization problem. The algorithm is initialized with multiple initial solutions, where each solution is obtained by dividing the normalized channel gain value, representing the channel gain over the noise power. Despite the nonconvex nature of the problem, Algorithm 1 consistently converges to the exact solution for different initial points. This indicates the existence of a unique locally optimal solution, which is successfully identified by Algorithm 1.

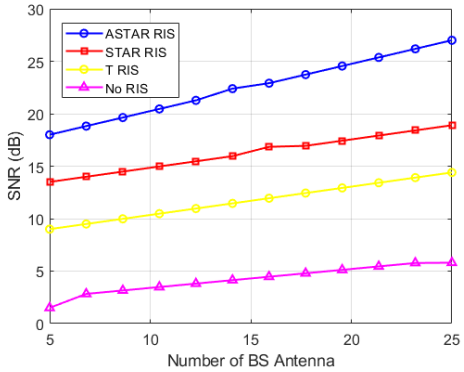

FIGURE 5: The change of SNR with number of BS antenna

Fig. 5 illustrates the SNR as a function of the number of mBS antennas across four scenarios: ASTAR RIS, STAR RIS, T RIS, and no RIS. The results highlight several key insights. Initially, as the number of transmit antennas at the BS is small, the SNR experiences a rapid increase. However, as the number of transmit antennas increases further, this growth becomes slower. This is attributed to the higher power consumption associated with a more significant number of antennas, leading to a reduced slope in improving SNR. Despite the diminishing returns in SNR improvement with increased antennas, ASTAR RIS consistently outperforms the other configurations, achieving the highest SNR across all antenna counts. This underscores the efficiency of ASTAR RIS in leveraging both active and passive beamforming for superior signal quality. Furthermore, the results highlight the trade-offs between performance and power consumption, where ASTAR RIS provides a robust solution for scenarios demanding high SNR, albeit with higher energy requirements. Conversely, STAR RIS and T RIS present viable alternatives for systems prioritizing energy efficiency while benefiting from RIS-assisted improvements.

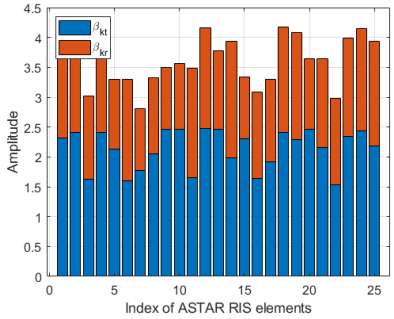

FIGURE 6: ASTAR element transmission and reflection amplitudes

This article has been accepted for publication in IEEE Open Journal of Vehicular Technology. This is the author's version which has not been fully edited and content may change prior to final publication. Citation information: DOI 10.1109/OJVT.2024.3509736 IEEE Open Journal of Vehicular Technology

Fig. 6 shows the distribution of transmission and reflection amplitudes among the ASTAR RIS elements, denoted as β_{kt} and β_{kr}, respectively. The results reveal a consistent trend where more energy is allocated to transmission amplitudes than reflection amplitudes. This allocation strategy stems from considering weaker channel gains, which necessitate higher amplitudes to achieve a desirable SNR for each user. The emphasis on transmission amplitudes is particularly crucial in scenarios where the direct transmission path is more dominant in improving the system's performance. The ASTAR RIS system effectively enhances signal quality and network efficiency by dynamically adjusting the amplitude allocation. Consequently, the ASTAR-RIS system optimizes the energy allocation by prioritizing transmission amplitudes, significantly improving SNR and ensuring robust communication performance even in challenging channel conditions.

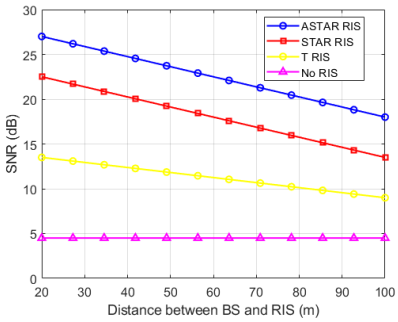

FIGURE 7: The effect of BS-ASTAR RIS distance on SNR

Fig. 7 provides insights into the relationship between SNR and the distance between the ASTAR-RIS and the mBS and then compares it with benchmark schemes. The SNR is a key performance metric that measures the quality of the received signal relative to the background noise. In this case, the SNR is influenced by the spatial positioning of the ASTAR-RIS concerning the BS. The SNR decreases as the distance between the ASTAR-RIS and the BS increases. This phenomenon can be attributed to the characteristics of the cascaded channel. The cascaded channel is relatively large when the RISs are positioned near the BS, resulting in a higher SNR. However, as the distance between the ASTAR-RIS and the BS increases, the cascaded channel experiences more attenuation, leading to decreased SNR. These results demonstrate the sensitivity of SNR to RIS placement, underscoring the need for careful deployment in practical scenarios. Additionally, ASTAR-RIS consistently achieves a higher SNR than other configurations, showcasing its robustness against distance-induced attenuation.

The relationship between the SNR and the number of ASTAR RIS is illustrated in Fig 8. Increasing the ASTAR RIS leads to a consistent improvement in SNR for the proposed model. This improvement is attributed to the higher SNR achieved by employing more ASTAR elements and ASTAR-

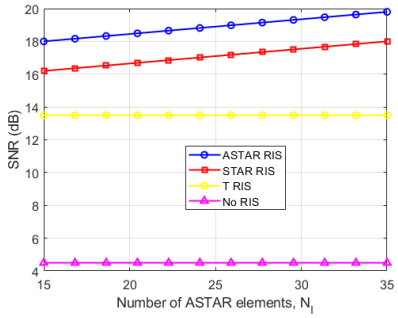

FIGURE 8: SNR changing over various ASTAR elements

RISs. Consequently, the system demonstrates enhanced SNR. Furthermore, the SNR exhibits a more pronounced increase with the number of RISs compared to the number of ASTAR elements, highlighting the more excellent SNR benefits of deploying ASTAR RIS. These results emphasize that scaling the number of ASTAR elements is a key design strategy to maximize system performance. ASTAR RIS outperforms other configurations, reinforcing its superior capability in enhancing signal quality while maintaining power efficiency.

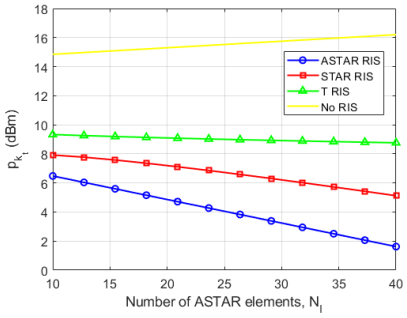

FIGURE 9: p_{k_t} changing for various N_1

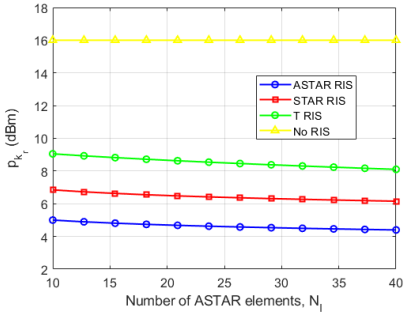

FIGURE 10: p_{k_r} changing for various N_1

Fig. 9 and Fig. 10 illustrate the variations in transmission power and reflection power, respectively, across different numbers of ASTAR elements. When no RIS is incorporated into the model, the power levels are observed to be

high. Additionally, the power required for STAR RIS is higher than ASTAR RIS. These observations highlight the efficiency of the proposed model, which aims to maximize system performance while minimizing power consumption. The findings suggest that by leveraging the ASTAR-RIS approach, the proposed model achieves an optimal balance between transmission and reflection power, leading to enhanced system efficiency. By reducing power requirements and effectively managing RIS elements, the proposed model demonstrates its potential to optimize system performance while ensuring energy-efficient operation. The results indicate that the ASTAR RIS configuration consistently achieves lower power consumption than other RIS setups, underscoring its energy efficiency advantages. The findings suggest that by leveraging the ASTAR-RIS approach, the proposed model achieves an optimal balance between transmission and reflection power, leading to enhanced system efficiency. This balance is particularly significant in large-scale deployments where power management is crucial.

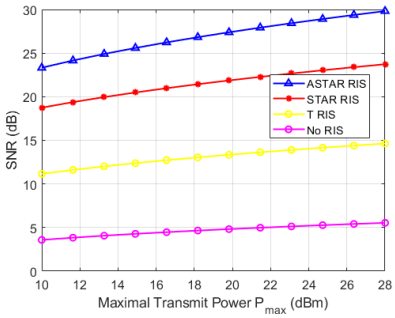

FIGURE 11: SNR changing over maximum transmit power

Fig. 11 presents the results where we examine the impact of varying the mBS transmit power on the SNR. By comparing the performance of the proposed scheme with the benchmark schemes, we observe that the scheme consistently achieves a higher SNR value. This suggests that the proposed scheme offers improved signal quality and performance than benchmark schemes. Furthermore, as we increase the mBS transmit power, we observe a corresponding increase in the SNR. This relationship indicates that higher transmit power levels contribute to improved signal strength and enhanced SNR. It implies that increasing the power of the mBS can lead to better signal reception and potentially enhanced system performance. The further highlight that the ASTAR RIS configuration achieves superior SNR improvements at all power levels, demonstrating its robustness even under varying power constraints. This insight underscores the proposed model's ability to capitalize on higher transmit powers, ensuring better signal reception and enhanced system performance while maintaining energy efficiency.

Fig.12 and Fig 13 illustrate the performance of ASTAR-RIS, STAR-RIS, and T-RIS regarding SNR and power consumption over multiple iterations. ASTAR-RIS demonstrates

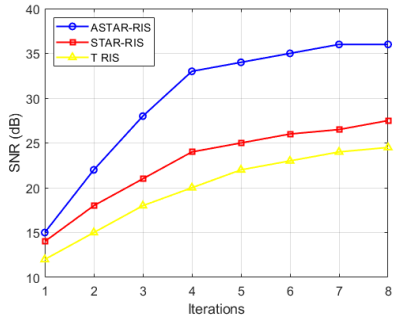

FIGURE 12: SNR changing over iterations

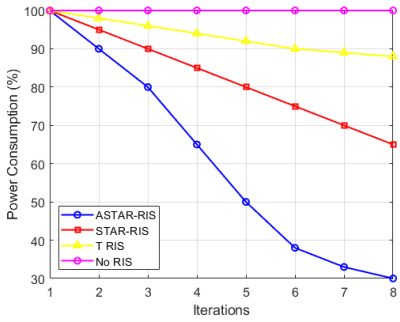

FIGURE 13: Power consumption over iterations

the highest SNR gain, reaching nearly 40 dB after eight iterations, significantly outperforming STAR-RIS and T-RIS. Regarding power consumption, ASTAR-RIS shows a notable decrease, reducing its power usage to 50%, while STAR-RIS experiences a moderate reduction. On the other hand, T-RIS maintains constant power consumption across all iterations, highlighting the efficiency advantages of ASTAR-RIS. In contrast, T-RIS maintains constant power consumption across all iterations, emphasizing its limited adaptability to dynamic system requirements. These results highlight the dual advantage of ASTAR-RIS in achieving superior SNR gains while simultaneously optimizing energy efficiency, making it a highly effective solution for modern communication systems.

In this study, we account for interfering user signals across different cells, reflecting real-world multi-cell network environments more accurately. In practice, user signals across cells often interfere with each other, especially in dense deployments with multiple STAR-RIS units. In such scenarios, inter-cell interference management becomes critical to maintaining system performance. Coordination strategies, such as distributed beamforming or coordinated multipoint transmission, can synchronize the operations of multiple STAR-RIS units, minimizing interference and optimizing signal quality. Deploying a single STAR-RIS unit simplifies inter-cell interference management since the control over phase shifts and beamforming vectors is centralized. However, even in this case, interference from neighboring

cells can significantly impact performance. Power control mechanisms, scheduling, and frequency reuse techniques can be employed to mitigate these effects. Furthermore, advanced interference alignment techniques could enhance system robustness in the presence of interfering users. Future work should focus on evaluating the impact of inter-cell interference in multi-cell scenarios involving multiple STAR-RIS units and exploring optimized coordination strategies to mitigate such interference effectively.

VIII. Conclusions

In this paper, we propose a novel concept of ASTAR-RISs that amplify and reflect the mBS signals to enhance the quality of service in complex channel environments. ScNs integrated with ASTAR-RISs may be a promising solution to meet the growing demand for high-speed data transmission. ASTAR-RISs can exploit a propagation space of 360^0 or reflect/transmit signals with amplification and reflection properties. In the proposed model, these ASTAR-RISs serve as ScNs and are distributed to serve multiple users in transmission and reflection regions within ScNs. We develop optimal hybrid beamforming for users at the mBS using the multiple-input-multiple-output technique while dynamically controlling the energy consumption of the ASTAR-RIS. We propose an efficient model that ensures signal-to-noise ratio fairness for all users and minimizes overall power consumption while meeting user rate and phase shift constraints. We formulate a max-min optimization problem that optimizes the SNR and power consumption, subject to the ON/OFF status, phase shift, hybrid beamforming, and power budget of the ASTAR-RIS. The proposed approach involves two transmission schemes, and we use an alternating optimization algorithm to optimize the phase shift matrix at the ASTAR-RIS and the hybrid beamforming at the mBS. The phase optimization problem is solved using a successive convex approximation method that provides a closed-form solution at each step. The ASTAR-RIS's optimal ON/OFF status is determined using the dual method. Our simulation results demonstrate that the proposed approach significantly outperforms traditional RIS schemes. We plan to address this more complex modeling in future work, exploring more detailed models that account for the variation in energy consumption based on different amplification levels and real-time network conditions.

REFERENCES

[1] M. Adhikari and A. Hazra, "6G enabled ultra-reliable low-latency communication in edge networks," *IEEE Communications Standards Magazine*, vol. 6, no. 1, pp. 67–74, 2022.

[2] Z. Gao, L. Dai, D. Mi, Z. Wang, M. A. Imran, and M. Z. Shakir, "mmWave massive-MIMO-based wireless backhaul for the 5G ultra-dense network," *IEEE Wireless Communications*, vol. 22, no. 5, pp. 13–21, 2015.

[3] S. Ahmed, A. E. Kamal, M. Y. Selim, S. R. Sabuj, and M. Hamamura, "Revolutionizing batteryless iot systems to enhance nonlinear energy harvesting using RIS active and passive elements," *IEEE Open Journal of the Communications Society*, pp. 1–1, 2024.

[4] Y. Chen, Y. Wang, Z. Wang, and P. Zhang, "Robust beamforming for active reconfigurable intelligent omni-surface in vehicular communications," *IEEE Journal on Selected Areas in Communications*, vol. 40, no. 10, pp. 3086–3103, 2022.

[5] Y. Pan, C. Pan, S. Jin, and J. Wang, "RIS-aided near-field localization and channel estimation for the terahertz system," *IEEE Journal of Selected Topics in Signal Processing*, vol. 17, no. 4, pp. 878–892, 2023.

[6] T. H. Nguyen and T. T. Nguyen, "On performance of STAR-RIS-enabled multiple two-way full-duplex D2D communication systems," *IEEE Access*, vol. 10, pp. 89 063–89 071, 2022.

[7] J. Zhao, Y. Zhu, X. Mu, K. Cai, Y. Liu, and L. Hanzo, "Simultaneously transmitting and reflecting reconfigurable intelligent surface (STAR-RIS) assisted UAV communications," *IEEE Journal on Selected Areas in Communications*, vol. 40, no. 10, pp. 3041–3056, 2022.

[8] S. Abeywickrama, R. Zhang, Q. Wu, and C. Yuen, "Intelligent reflecting surface: Practical phase shift model and beamforming optimization," *IEEE Transactions on Communications*, vol. 68, no. 9, pp. 5849–5863, 2020.

[9] X. Mu, Y. Liu, L. Guo, J. Lin, and R. Schober, "Simultaneously transmitting and reflecting (STAR) RIS aided wireless communications," *IEEE Transactions on Wireless Communications*, vol. 21, no. 5, pp. 3083–3098, 2022.

[10] J. Xu, Y. Liu, X. Mu, and O. A. Dobre, "Star-riss: Simultaneous transmitting and reflecting reconfigurable intelligent surfaces," *IEEE Communications Letters*, vol. 25, no. 9, pp. 3134–3138, 2021.

[11] Y. Liu, X. Mu, J. Xu, R. Schober, Y. Hao, H. V. Poor, and L. Hanzo, "Star: Simultaneous transmission and reflection for 360° coverage by intelligent surfaces," *IEEE Wireless Communications*, vol. 28, no. 6, pp. 102–109, 2021.

[12] Z. Zhang, L. Song, Z. Han, and W. Saad, "Coalitional games with overlapping coalitions for interference management in small cell networks," *IEEE Transactions on Wireless Communications*, vol. 13, no. 5, pp. 2659–2669, 2014.

[13] A. Liu, V. K. Lau, L. Ruan, J. Chen, and D. Xiao, "Hierarchical radio resource optimization for heterogeneous networks with enhanced inter-cell interference coordination (eICIC)," *IEEE Transactions on signal processing*, vol. 62, no. 7, pp. 1684–1693, 2014.

[14] D. López-Pérez, A. Valcarce, G. De La Roche, and J. Zhang, "Ofdma femtocells: A roadmap on interference avoidance," *IEEE communications magazine*, vol. 47, no. 9, pp. 41–48, 2009.

[15] N. Saquib, E. Hossain, and D. I. Kim, "Fractional frequency reuse for interference management in lte-advanced hetnets," *IEEE Wireless Communications*, vol. 20, no. 2, pp. 113–122, 2013.

[16] V. Chandrasekhar, J. G. Andrews, T. Muharemovic, Z. Shen, and A. Gatherer, "Power control in two-tier femtocell networks," *IEEE Transactions on Wireless Communications*, vol. 8, no. 8, pp. 4316–4328, 2009.

[17] J. Xiao, C. Yang, A. Anpalagan, Q. Ni, and M. Guizani, "Joint interference management in ultra-dense small-cell networks: A multi-domain coordination perspective," *IEEE Transactions on Communications*, vol. 66, no. 11, pp. 5470–5481, 2018.

[18] R. Tao, W. Liu, X. Chu, and J. Zhang, "An energy saving small cell sleeping mechanism with cell range expansion in heterogeneous networks," *IEEE Transactions on Wireless Communications*, vol. 18, no. 5, pp. 2451–2463, 2019.

[19] Y. Sun, R. P. Jover, and X. Wang, "Uplink interference mitigation for ofdma femtocell networks," *IEEE Transactions on Wireless Communications*, vol. 11, no. 2, pp. 614–625, 2011.

[20] A. Adhikary and G. Caire, "On the coexistence of macrocell spatial multiplexing and cognitive femtocells," in *2012 IEEE International Conference on Communications (ICC)*. IEEE, 2012, pp. 6830–6834.

[21] N. DOCOMO, "Docomo conducts world's first successful trial of transparent dynamic metasurface," 2020.

[22] J. Zhang, Z. Li, L. Shao, and W. Zhu, "Dynamical absorption manipulation in a graphene-based optically transparent and flexible metasurface," *Carbon*, vol. 176, pp. 374–382, 2021.

[23] X. Wang, J. Ding, B. Zheng, S. An, G. Zhai, and H. Zhang, "Simultaneous realization of anomalous reflection and transmission at two frequencies using bi-functional metasurfaces," *Scientific reports*, vol. 8, no. 1, pp. 1–8, 2018.

[24] C. Wu, Y. Liu, X. Mu, X. Gu, and O. A. Dobre, "Coverage characterization of star-ris networks: NOMA and OMA," *IEEE Communications Letters*, vol. 25, no. 9, pp. 3036–3040, 2021.

[25] S. Zhang, H. Zhang, B. Di, Y. Tan, Z. Han, and L. Song, "Beyond intelligent reflecting surfaces: Reflective-transmissive metasurface aided communications for full-dimensional coverage extension," *IEEE Transactions on Vehicular Technology*, vol. 69, no. 11, pp. 13 905–13 909, 2020.

[26] M. Fu, Y. Zhou, Y. Shi, and K. B. Letaief, "Reconfigurable intelligent surface empowered downlink non-orthogonal multiple access," *IEEE Transactions on Communications*, vol. 69, no. 6, pp. 3802–3817, 2021.

[27] Y. Li, M. Jiang, Q. Zhang, and J. Qin, "Joint beamforming design in multi-cluster MISO NOMA reconfigurable intelligent surface-aided downlink communication networks," *IEEE Transactions on Communications*, vol. 69, no. 1, pp. 664–674, 2020.

[28] J. Zhu, Y. Huang, J. Wang, K. Navaie, and Z. Ding, "Power efficient irs-assisted noma," *IEEE Transactions on Communications*, vol. 69, no. 2, pp. 900–913, 2020.

[29] Z. Zhang, Y. Cui, F. Yang, and L. Ding, "Analysis and optimization of outage probability in multi-intelligent reflecting surface-assisted systems," *arXiv preprint arXiv:1909.02193*, 2019.

[30] P. Wang, J. Fang, X. Yuan, Z. Chen, and H. Li, "Intelligent reflecting surface-assisted millimeter wave communications: Joint active and passive precoding design," *IEEE Transactions on Vehicular Technology*, vol. 69, no. 12, pp. 14 960–14 973, 2020.

[31] C. Huang, Z. Yang, G. C. Alexandropoulos, K. Xiong, L. Wei, C. Yuen, and Z. Zhang, "Hybrid beamforming for ris-empowered multi-hop terahertz communications: A DRL-based method," in *2020 IEEE Globecom Workshops (GC Wkshps)*. IEEE, 2020, pp. 1–6.

[32] M. A. Saeidi, M. J. Emadi, H. Masoumi, M. R. Mili, D. W. K. Ng, and I. Krikidis, "Weighted sum-rate maximization for multi-irs-assisted full-duplex systems with hardware impairments," *IEEE Transactions on Cognitive Communications and Networking*, vol. 7, no. 2, pp. 466–481, 2021.

[33] Q. Wu and R. Zhang, "Intelligent reflecting surface enhanced wireless network via joint active and passive beamforming," *IEEE Transactions on Wireless Communications*, vol. 18, no. 11, pp. 5394–5409, 2019.

[34] C. Huang, A. Zappone, G. C. Alexandropoulos, M. Debbah, and C. Yuen, "Reconfigurable intelligent surfaces for energy efficiency in wireless communication," *IEEE Transactions on Wireless Communications*, vol. 18, no. 8, pp. 4157–4170, 2019.

[35] S. Hua, Y. Zhou, K. Yang, Y. Shi, and K. Wang, "Reconfigurable intelligent surface for green edge inference," *IEEE Transactions on Green Communications and Networking*, vol. 5, no. 2, pp. 964–979, 2021.

[36] Y. Tang, G. Ma, H. Xie, J. Xu, and X. Han, "Joint transmit and reflective beamforming design for IRS-assisted multiuser MISO SWIPT systems," in *ICC 2020-2020 IEEE International Conference on Communications (ICC)*. IEEE, 2020, pp. 1–6.

[37] Y. Sun, J. Xu, and W. Yang, "Joint active and passive beamforming design for the reconfigurable intelligent surface-aided miso system," *IEEE Transactions on Wireless Communications*, vol. 19, no. 8, pp. 4878–4890, 2020.

[38] Y. Liang, R. Zhao, and Q. Wu, "Intelligent reflecting surface enhanced wireless network: Joint active and passive beamforming design," *IEEE Transactions on Wireless Communications*, vol. 18, no. 11, pp. 5620–5632, 2019.

[39] Q.-U.-A. Nadeem, A. Kammoun, A. Chaaban, M. Debbah, and M.-S. Alouini, "Asymptotic max-min SINR analysis of reconfigurable intelligent surface assisted MISO systems," *IEEE Transactions on Wireless Communications*, vol. 19, no. 12, pp. 7748–7764, 2020.

[40] X. Liu, Y. Yu, F. Li, and T. S. Durrani, "Throughput maximization for RIS-UAV relaying communications," *IEEE Transactions on Intelligent Transportation Systems*, vol. 23, no. 10, pp. 19 569–19 574, 2022.

[41] S. Zhang, H. Zhang, B. Di, Y. Tan, Z. Han, and L. Song, "Beyond intelligent reflecting surfaces: Reflective-transmissive metasurface aided communications for full-dimensional coverage extension," *IEEE Transactions on Vehicular Technology*, vol. 69, no. 11, pp. 13 905–13 909, 2020.

[42] I. Yildirim, A. Uyrus, and E. Basar, "Modeling and analysis of reconfigurable intelligent surfaces for indoor and outdoor applications in future wireless networks," *IEEE Transactions on Communications*, vol. 69, no. 2, pp. 1290–1301, 2021.

[43] M. Fu, Y. Zhou, and Y. Shi, "Intelligent reflecting surface for downlink non-orthogonal multiple access networks," in *2019 IEEE Globecom Workshops (GC Wkshps)*, 2019, pp. 1–6.

[44] S. Zhou, W. Xu, K. Wang, M. Di Renzo, and M.-S. Alouini, "Spectral and energy efficiency of IRS-assisted MISO communication with hardware impairments," *IEEE wireless communications letters*, vol. 9, no. 9, pp. 1366–1369, 2020.

[45] L. Vandenberghe, "Convex optimization techniques in system identification," *IFAC Proceedings Volumes*, vol. 45, no. 16, pp. 71–76, 2012.

[46] Y. Chen, Y. Wang, and L. Jiao, "Robust transmission for reconfigurable intelligent surface aided millimeter wave vehicular communications with statistical CSI," *IEEE Transactions on Wireless Communications*, vol. 21, no. 2, pp. 928–944, 2022.